TECHNISCHE
UNIVERSITÄT
WIEN
Vienna University of Technology

INSTITUT FÜR
MECHANIK UND
MECHATRONIK
Mechanics & Mechatronics

DIPLOMARBEIT

Regelung eines Compound-Split-Antriebsstrangs mit aktiver Schwingungsdämpfung

ausgeführt zum Zwecke der Erlangung des akademischen Grades eines Diplom-Ingenieurs
unter der Leitung von

Ao.Univ.Prof. Dipl.-Ing. Dr.techn. Martin Kozek
Dipl.-Ing. Agnes Poks
Institut für Mechanik und Mechatronik
Abteilung für Regelungstechnik und Prozessautomatisierung

eingereicht an der Technischen Universität Wien

Fakultät für Maschinenwesen und Betriebswissenschaften

von

Benjamin Pommer
[redacted]

Wien, am 16. August 2023

Benjamin Pommer

Eidesstattliche Erklärung

Ich erkläre eidesstattlich, dass ich die Arbeit selbständig angefertigt, keine anderen als die angegebenen Hilfsmittel benutzt und alle aus ungedruckten Quellen, gedruckter Literatur oder aus dem Internet im Wortlaut oder im wesentlichen Inhalt übernommenen Formulierungen und Konzepte gemäß den Richtlinien wissenschaftlicher Arbeiten zitiert, durch Fußnoten gekennzeichnet bzw. mit genauer Quellenangabe kenntlich gemacht habe.

Wien, am 16. August 2023 Your Name

Danksagung

An dieser Stelle will ich ein paar Worte des Dankes an die Menschen richten, die mir den Abschluss ermöglicht haben bzw. mich dabei unterstützt haben. An erster Stelle will ich meinen Eltern danken, die trotz der Widrigkeiten, mich in jungen Jahren hingehend gefördert haben, um den Grundstein für meine akademische Laufbahn errichtet hatten.
Der Vielzahl an Studienkollegen, die bereits absolviert haben, noch absolvieren werden oder ihr Studium abgebrochen haben gebührt Dank für den fachlichen und den außerfachlichen Austausch unabhängig davon, ob noch Freundschaft, Bekanntschaft oder Kontakt besteht oder nicht.
Besonders hervorzuheben sind die Studienkollegen, die sich ehrenamtlich bei der Fachschaft für Maschinenbau engagieren und sich für ihre Mitstudierenden in vielerlei Hinsicht einsetzen.
Schließlich spreche ich dem leitenden Professor dieser Diplomarbeit, Martin Kozek, meinen Dank aus, der an den entscheidenden Stellen die Weichen für einen gelungenen Abschluss entsprechend gestellt hat.

Kurzfassung

Im Rahmen des Forschungsprojektes VARI-SPEED zu Drehflüglern mit variabler Rotordrehzahl ergab sich die Notwendigkeit ein ausgereiftes Regelungskonzept zu entwickeln, das sich vor allem durch Robustheit auszeichnet. Die Grundlage einer solchen Regelung ist eine fundierte Modellbildung, bei der die wesentlichen physikalischen Eigenschaften in die Systembeschreibung fließen ohne zu sehr in Konflikt mit den Validierungsdaten zu kommen.
Die Modellierung und Regelung eines Helikopters, im Speziellen eines UH-60, führt einen vor die Herausforderung eines höhergradig nicht-linearen Systems, dessen Systemdynamiken sich mit einer Menge an Parametern ändert. Daneben sind von der Natur oder konkret von den Besonderheiten des technischen Systems gestellte Randbedingungen beim Reglerentwurf zu beachten.
Unter Einhaltung des Ähnlichkeitsprinzips im Rahmen der Modellbildung wurde ein Hybridgetriebe für Kraftfahrzeuge gewählt, das als vereinfachte Basis für den Reglerentwurf seinen Dienst erbracht hat. Als Reglerungsalgorithmus überzeugte der Fuzzy-MPC als geeigneter Kandidat und erzielte zufriedenstellende Ergebnisse für die vorliegende Aufgabenstellung.

Abstract

Within the framework of the VARI-SPEED research project on rotorcraft with variable rotor speed, the necessity arose to develop a technically mature control concept that is characterised above all by robustness. The basis of such a control system is a well-founded modelling, in which the essential physical properties flow into the system description without coming too much into conflict with the validation data.
The modelling and control of a helicopter, in particular a UH-60, leads one to the challenge of a highly non-linear system whose system dynamics change with a set of parameters. In addition, boundary conditions imposed by nature or specifically by the peculiarities of the technical system must be taken into account when designing the controller.
In compliance with the principle of similarity in the context of modelling, a hybrid transmission for motor vehicles was chosen, which served as a simplified basis for the controller design. As a control algorithm, the fuzzy MPC is convinced as a suitable candidate and achieved satisfactory results for the given task.

Contents

Chapter 1

Introduction

1.1 Motivation

Until recent years, rotor-crafts were only designed for one particular operating point in terms of rotor speed. Subject-specific studies had shown that an extension from one operating point to an operating range, or in other words, by allowing a given helicopter to operate within a variable rotor speed opens up a variety of new possibilities. Reduction of the power demand, noise and greenhouse emission are the bountiful harvest of this promising technological innovation. Those benefits are not bound to a particular type of rotor-craft but its whole spectrum - tandem, tilt-rotor or standard configuration - can benefit from it [1, 2].
From 2015 until 2019, a funded scientific project - Development of a Variable Speed Rotor System or shortly VARISPEED - from TU München as a cooperation with the University of Technology Vienna and Zoerkler Gears GmbH & Co KG had been conducting an investigation of this promising potential, to develop suitable rotor blades and a transmission and an overall design of such a rotorcraft[3, 4].
A crucial factor for the development of that innovative technology was a suitable transmission which is able to transform a constant input rotational speed of the turbine into a variable one. Additionally, the rotorcraft system must have been able to perform in a variable operating regime of the rotational speed. Several aspects of the helicopter technology like the geometry of the rotor blades, its strength property and its dynamic properties in comparison to systems with constant rotational speed were essential for a sufficient understanding of the optimization potential of the technology. Furthermore, the economical and ecological gain of that technology was in danger due to upcoming conflicts regarding additional weights which could equalize its power benefits [5, 6].
The versatile benefits of that multi-annual scientific activity are conspicuous. In particular, the variation of the main frequency of the rotational speed of the helicopter enables a reactive handling of radical changes in the flight weight, such that the rotor blades are

able to operate in an optimal condition balancing drag force and buoyancy force. This leads to an overall efficiency of the innovative drive system. A significant reduction of fuel consumption leads to a reduction in carbon dioxide emission. This technological progression supports the achievement of the climate targets. Besides those pleasant ecological promises, additional effects can be observed in the noise reduction which, on the one hand, preserves the urban areas and, on the other hand, again decreases the negative interdependence with natural regions [1, 6].
In 2020, VARISPEED II was born, due to the feasible results of the precurser project, dedicating to the scientific investigation of drive train dynamics and flight characteristics of a helicopter with variable main rotor speed [7].

1.2 Problem Description

Within VariSpeed II, a series of tasks must be done to carry forward the research into finalization. The models for the individual parts of the rotor-craft have to be designed and less relevant parts shall be neglected to capture the system's behaviour as precise as necessary. Additionally, each of the single components interacts with each other. Unwanted side effects shall be identified and suppressed. Individual contemplation is not reasonable anymore, since due to the complexity of the interplay individual components give rise to certain dynamics. Especially, the exploration of the shifting process and its impact onto the drive-train and the rotor plays a crucial role [8].
To sum it up, a solid model is the foundation to apply system analysis later on. The system has to portray an appropriate image of the system dynamics of the physical entity. The findings of VARISPEED I fill the gap of knowledge for the modelling process [7] and support sufficient model simplifications.
Finally, the resulting helicopter model represents a complex non-linear system which requires more sophisticated control strategies. Nevertheless, a control method shall be applied which is as simple as possible in the scope of such an undertaking and is not to expensive in terms of computation costs. Additionally, robustness shall be the main concern of the control algorithm in order to secure passengers safety. Performance thereby is assigned a secondary role in that manner. For the active damping of the rotational vibration, the dynamical components´of the rotor-craft have to be identified, so that the task can be completed efficiently.
This problem represents an interdisciplinary problem of power engineering, design sciences and control engineering. The scientific findings have been gathered and have already been converted into a system model. The objective now is to finalize and simplify the modelling and design a robust controller for the non-linear system.
Due to a delayed submission of a well-functioning UH-60 rotor-craft model on the side

of the project partners, the modelling phase was not able to be carried out as planned. Therefore, an analogous model had to be taken into account. The Hybrid Synergy Drive was a eligible choice to fill this role due its similarity in terms of modelling.

1.3 Research Question

The following question are covered in the thesis:

1. Is it possible to design a FMPC for the rotor-craft model which performs along the defined operation space?

2. Does the implementation of inequality constraints allow feasible solutions for the FMPC?

3. Can one show stability for this FMPC by the framework of Lyapunov?

Chapter 2

Modelling

2.1 Modelling of the Rotor Model

For the modelling purposes, the UH-60A helicopter was taken as a reference framework which was a suitable choice for the latter validation due to the availability of data [9, 10]. This helicopter type is characterized by its twin engine single main rotor utility. However, the modelling of the rotor itself requires multiple competencies due to its complicated physical behaviour. Mainly, aerodynamic and structural effects need to be taken into account to model the rotorcraft system for which the investigation of transient behaviour is of higher interest [8].
The dynamical behaviour of the rotor characterizes the dynamics of the whole rotorcraft due to its vibration loads. Especially, the configuration of the rotor blades plays a crucial role for the flap, lag and torsional vibration behaviour [11].
The rotor blades have to be designed in that way that their harmonics don't coincide with the nominal rotational speed to prevent to prevent a resonance disaster [12].
Blade frequency tuning, the remedy of the first choice, allows adapting the material properties of the blades and include the usage of tuning masses to prevent an overlap of the natural frequencies of the rotor with the harmonics in the operating state. Air resonance is an additional hazard for the flight safety. In this case, higher harmonics are critical. An optimal distance between the frequency layout and the resonances are considered to be $\pm 10\%$ [13].
Due to these facts, the scope of the variable rotor speed is tightly limited [12] and has to bear operations of the rotational speed close to the harmonics [11]. Therefore, a crucial role is assigned to the blade design. Taking structural elasticity and vibrational dynamics into account, a structural optimization for the rotor blades was conducted [14]. Especially, the effects of manufacturing uncertainties and their influence on rotational natural frequencies had to be investigated separately [15].
In order to analyse the dynamical behaviour, the rotor model was simulated by Dymore

which enable processing multibody sytems and features one and two dimensional finite element representations [9].
The model was validated in the operating regimes hover and forward flight against the wind tunnel data from NASA Ames 80 x 120ft test facility and data of flight tests from airloads flight test counter 85 [16].
Fig. 2.1 illustrates the multibody representation of the UH-60A main rotor system. The points in the multibody model are being measured in their own local body-frame coordinates rather than in the inertial coordinates. Revolute joints link the rotor model to the fuselage. Servos allow elastic movement along the local x-direction. Spherical joints allow isostatic conditions between the swash plate and the servos. The shaft is attached to the rotor hub at its upper end.
The elastomeric bearing models the flap, lead-lag and the feathering motion and serves as a connection between the blade retention and the rotor hub. The main rotor hub is modelled as a rigid body. The rotor blades are represented by beam elements and elastically attached to the rotor retention [5, 6, 9].
For the final rotor model, further model assumptions were made. Besides simplifications in the joints and lag dampers, the rotor blades were modelled to be rigid bodies. Validations of the simplified model justify the proposed assumptions [7]. In the scope of system identification of a simulation model of the simplified rotor model of [7], only lag vibrations of lower harmonics were assumed to be a threat in regards of the resonance disaster. Flap and torsional vibrations were fully neglected as well as higher harmonics of the lag vibrations. Additionally, the tail rotor was excluded in the modelling.
The rotor model itself is a non-linear SISO model which whose dynamics changes according to the flight state. The flight state is determined by the parameters rotational speed, the altitude of the helicopter represented by the respective air density and the forward velocity which form a three-dimensional parameter space which are a consequence of the system disturbances, flight controls from the pilot - collective and cycle and he system input, the mast torque which is a representation of the inner dynamics of the helicopter. The rotational speed is a parameter and the system output at the same time. This in total, constitutes the starting basis of the control design.

2.2 Modelling of the drive-train

The drive-train of the designed rotor-craft consists of two components - the GE T700 power turbine and the variator which are coordinated by a compound split transmission. The inert power turbine is supposed to provide rotational speed around its design value of 20900 rpm. The variator saves or provides excess energy and deals with the power demand of the helicopter in transient operation states of the system[8].

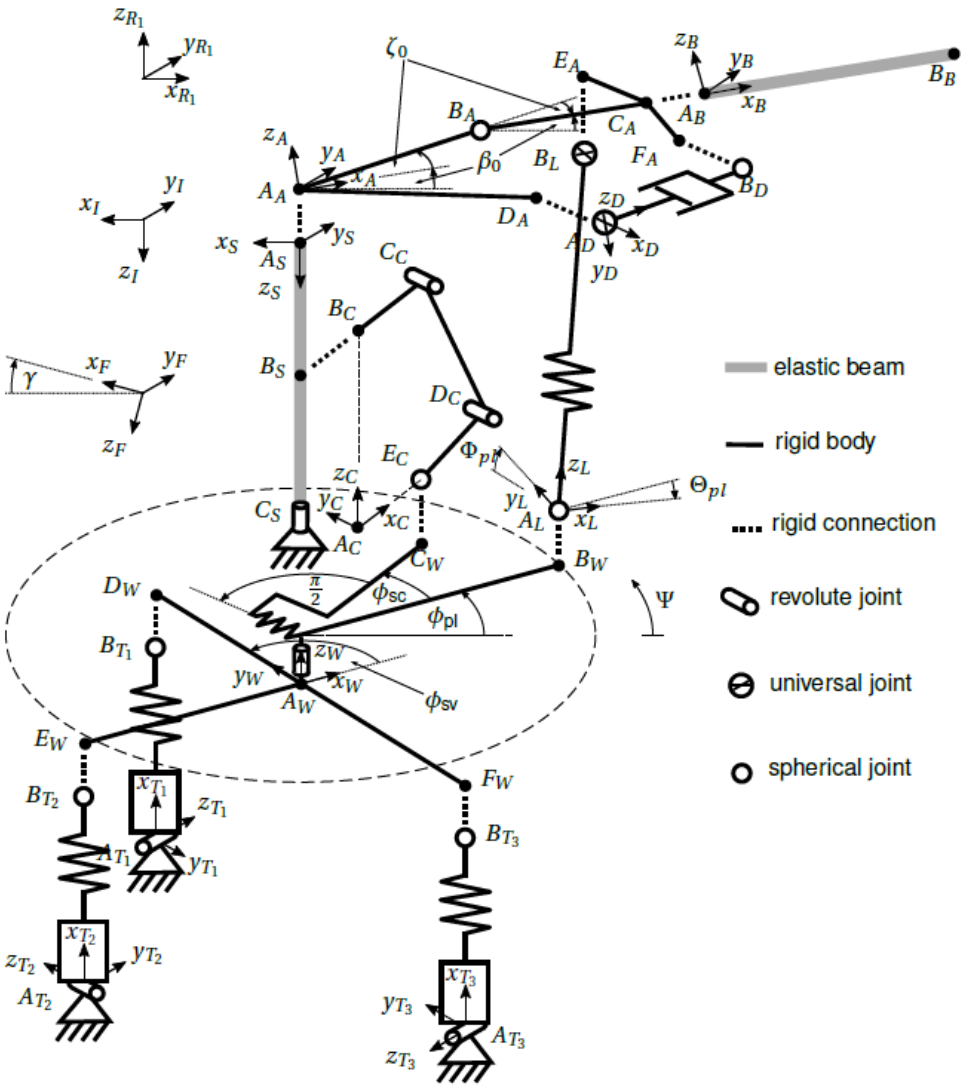

Figure 2.1: The Rotor Model as Multi-body representation in the scope of Finite Elements Methods. For simplification purposes, only one out of four blades are depicted. For each machine element, an individual coordinate system is defined within which the position of each part is described [5, 6, 9].

2.2.1 The GE T700 turboshaft engine

The leading principle of the 1300 kW power class two-shaft engine is a balanced interplay of a gas generator and a free power turbine. The turbo shaft engine is mechanically connected by linkages and gears to the input module of the transmission. Finally, the transmission links the GE T700, the variator and the rotor with each other. A freewheeling clutch ensures a one-sided drive flow from the turbine to the rotor system and blocks vice versa [8].
The GE T700 is modelled for a design point based on the research of VARISPEED I and operates through the following principle: The air is drawn in from the environment to the inlet and is sent from there to the compressor. An air plenum is located between the compressor and the combustor. The here occurring pressure fluctuations are not modelled. The heat supply to the combustor is modelled to be isobar. In the gas generator, the hot gas is expanded. In the second air plenum, a subset of the sucked in air is added and participates in the energy conversion. The hot gas is expanded in the power turbine. In the final step, the flow velocity is delayed [17].
The GE T700 was modelled for the design point

- $N_{P100} = 20900\ \frac{U}{min}$,
- $N_{G100} = 44700\ \frac{U}{min}$,
- $Q_{req} = 613$ Nm,
- $m_{F100} = 0.103\ \frac{kg}{s}$.

The model allows a variation of the rotational speed of the gas generator between 65% and 110% and of the rotational speed of the power turbine between 80% and 120%. A schematic block diagram of the modelled components of the GE T700 is found in Fig. 2.2. An important aspect of the the modelling procedure for the latter processing in regards of controller design is that the principle of conservation of angular momentum is utilized to cover the transient behaviour of the gas generator and the free turbine which results in a set of first order ordinary differential equations [8].
The remaining algebraic equations only constitute a control gain from a control engineering perspective. The input of its plant model is the fuel flow in [kg/s]. The disturbance is considered to be the required torque by the drive-train in [Nm] and the output is set to be the rotational speed of the power turbine in [rpm].

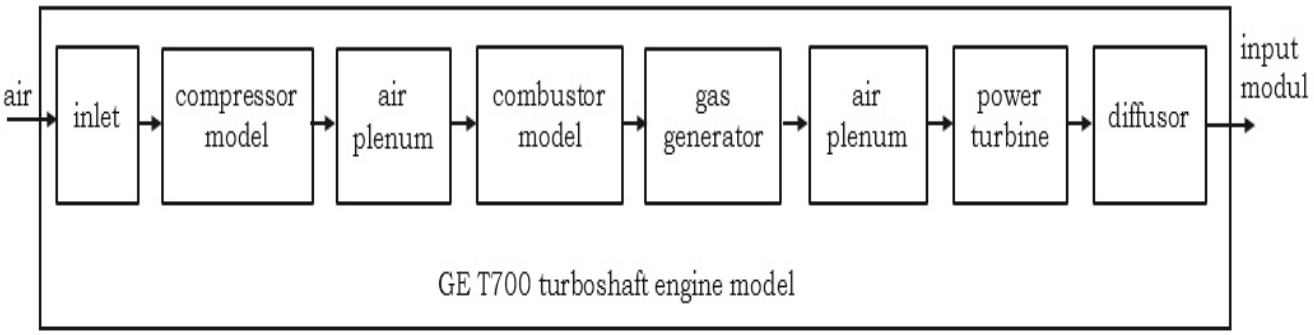

Figure 2.2: Schematic block diagram of the modelled components of the GE T700 turbine [17]

Control of the GE T700

It was intended to be controlled by a PID controller combined with a feed-forward control. This improves the tracking behaviour of the closed loop system by leading the set-point value directly onto the input of the plant [18, 19]. The PID controller was designed by the method of Chien-Hrones-Reswick for the aperiodic limit case with modelled disturbances which is a popular alternative method for Ziegler-Nichols and the T-sum rule [20].
Additionally, this hybrid control technique allows the system to react to changing set-point value [18]. Fig. 2.3 illustrates this control principle where $G_{FF}(s)$, $G_C(s)$, $G_Z(s)$ and $G_P(s)$ represent the feed-forward controller, the PID controller, the disturbance transfer function and the plant, respectively [19]. Since the poles of the set-point transfer function and the disturbance transfer function have the same denominator, no additional stability analysis has to be conducted [18]. The transfer function of the feed-forward controller

$$G_{FF}(s) = \frac{1}{G_P(s)} \tag{2.1}$$

is not valid for the following cases [18]:

1. If $G_P(s)$ has zeros in the right half plain of the s-domain then $G_{FF}(s)$ has unstable poles so that the whole system becomes unstable.

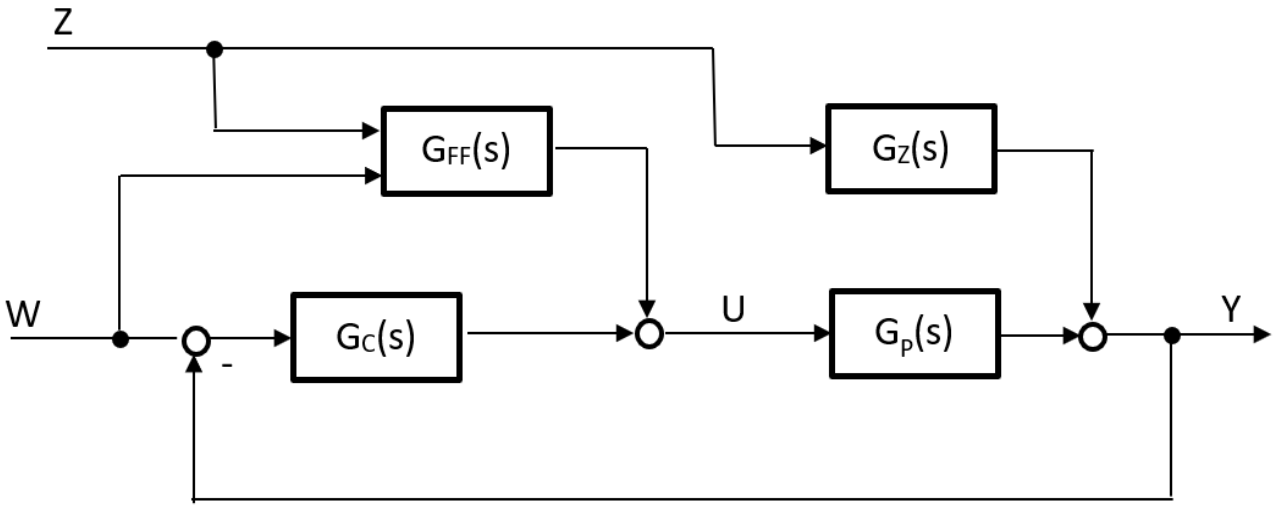

Figure 2.3: Block Diagram of a Two Degree of Freedom Control Scheme - PID and Feed-Forward Controller [19]

2. Unavoidable dead-time behaviour in plants require additional differentiating behaviour in $G_{FF}(s)$ which is generally inconvenient to conduct.

3. Inaccurate modelling in $G_P(s)$ can to further problems in $G_{FF}(s)$ [18].

Anyhow, since the underlying model of the GE T700 turbo shaft engine is not invertible, an alternative approach had to be performed. Instead of inverting the model, a look-up table was created. Therefore, the GE T700 simulation model was excited by a series of the steps inputs within the widest possible operating space in the simulation model. The received discrete input-output data was interpolated between its coarse nodes and could afterwards be inverted to yield the required polynomial which constitutes the feedback controller. Thereby, one receives set of constant compensations which make up an improvised feed-forward controller which is illustrated in Fig. 2.4.

Three different control scenarios using a series of various disturbance signals were conducted to evaluate the system behaviour. On each plot, the required torque, the fuel mass flow, the rotational speed of the free power turbine and the rotational speed of the gas generator are depicted and represent the system disturbance, the system input, the system output, respectively. The rotational speed of the gas generator is not assigned any primary role in a control systems context but its value must be verified not to

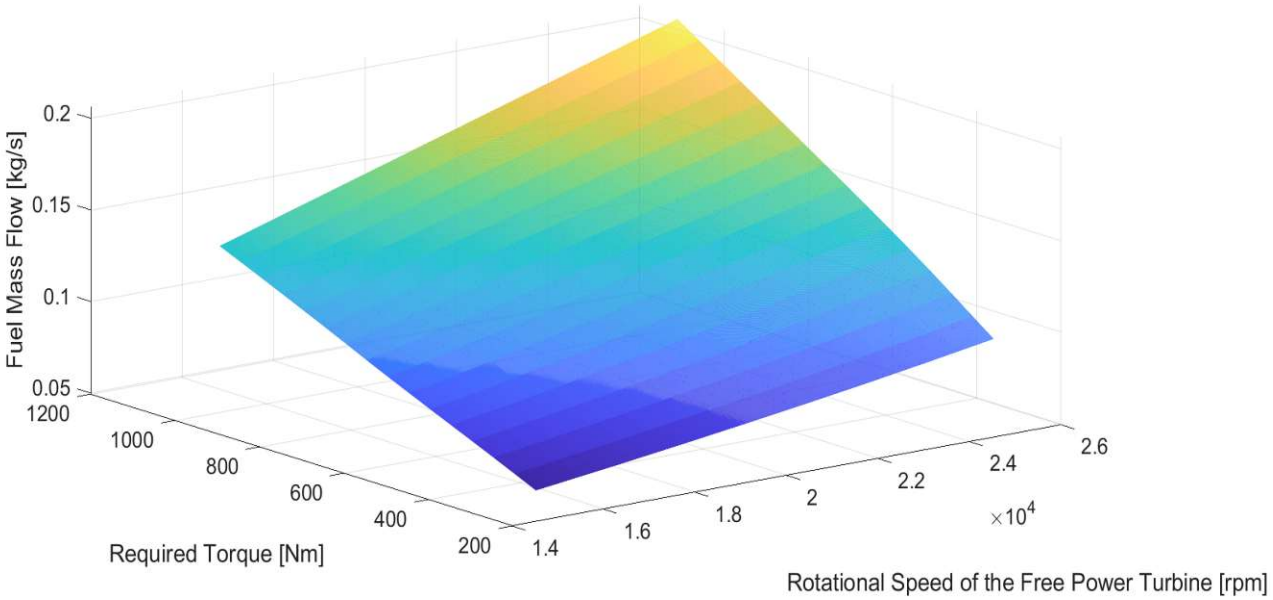

Figure 2.4: 3D Look-Up Table as a Generic Feed-Forward Controller for closed-loop GE T700 system. The fuel mass flow is mapped by the required torque and the rotational speed.

violate the boundaries of the operation range.
It was crucial for the validity of the power turbine model that the boundaries for the rotational speed of the free power turbine $15900U/min \leq N_P \leq 25900U/min$ and the rotational speed for the gas generator $29055U/min \leq N_G \leq 49170U/min$ are not violated and that the system remains stable. A series of periodic step signal, a cyclic step signal and a ramp signal were used as an excitation signal. The simulation results can be found in figure 2.5a, 2.5b and 2.5c.

Approximation of the GE T700 Model through Linear Regression

In order to enable convenient handling in a model-based predictive controller, the GE T700 model was approximated by a PT1 element, for which a multi-variable linear regression based on the required torque, the fuel mass flow and the rotational speed of the power turbine. This was done to obtain a description of the stationary part of the model.
The PT1 element is suitable as a convenient solution to approximate the inert dynamic behavior of the GE T700 turbine. The time constant of the PT1 element

$$\dot{x} = -\frac{x}{T} + \frac{x_{stat}}{T} \tag{2.2}$$

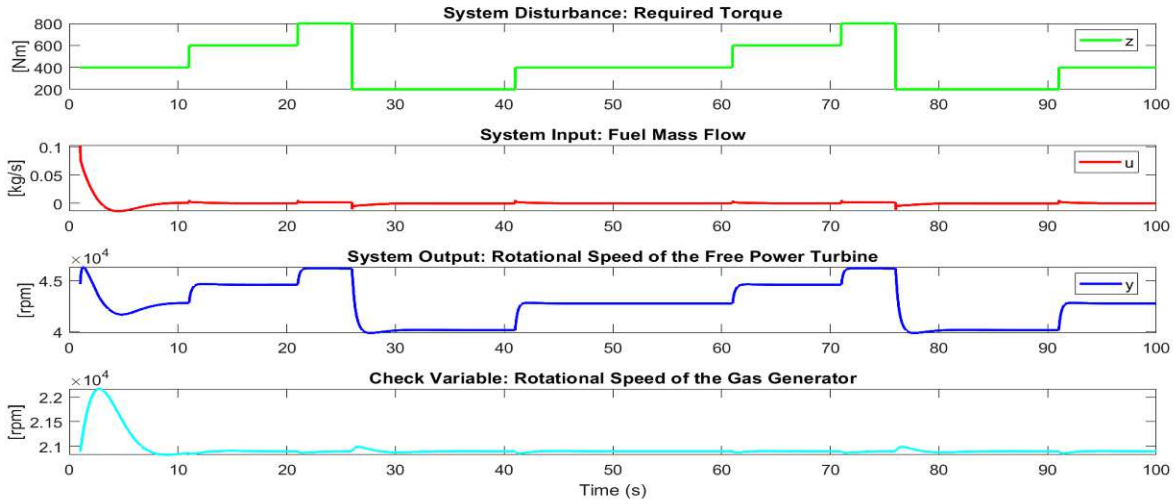

(a) Simulation Experiment 1: the closed-loop system (with a PID and Feedforward controller) was excited with a periodic step signal on the disturbance signal.

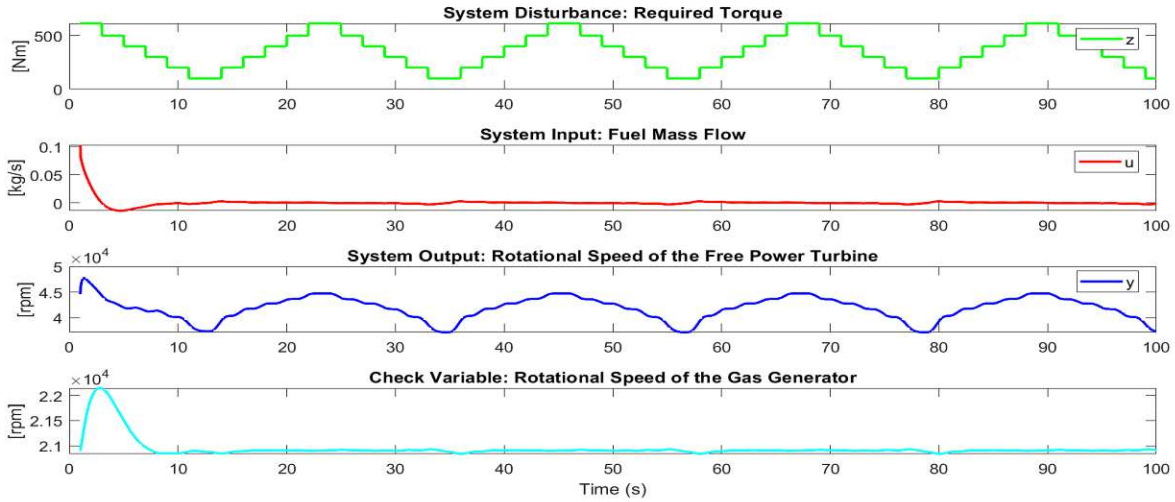

(b) Simulation Experiment 2: the closed-loop system (with a PID and Feedforward controller) was excited with a cyclic step signal on the disturbance signal.

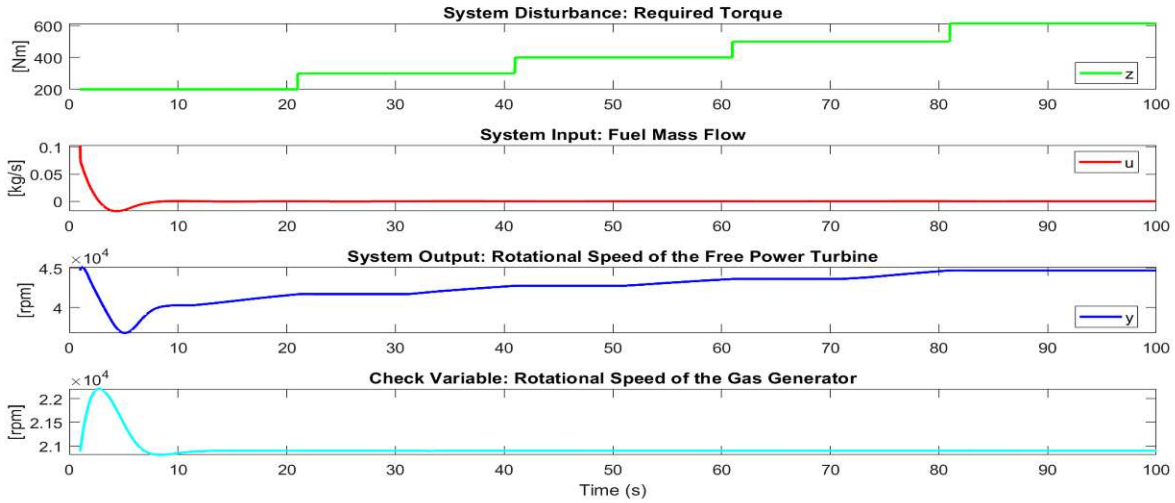

(c) Simulation Experiment 3: the closed-loop system (with a PID and Feedforward controller) was excited with a stepwise ramp signal on the disturbance signal.

was evaluated by the step response of the system and yields T = 15s. The static part was set to be the characteristic curve of the GE T700 model, which is illustrated in Figure 2.6. Therefore, the simulation model was excited with a series of steps regarding the system input - fuel mass flow - and the system disturbance - the required torque around the design point and the operating point of the turbo shaft engine. Finally, a multidimensional linear regression equation

$$x_{stat} = \beta_0 + \beta_1 x_{stat,1} + \beta_2 x_{stat,2} \tag{2.3}$$

is obtained where $\beta_0 = 5917.90\frac{1}{min}$, $\beta_1 = 260940.23\frac{s}{minkg}$ and $\beta_2 = -18.28\frac{1}{minNm}$. Now, equation 2.3 was augmented by an additive constant which facilitates the inclusion of the influence of external pressure, to yield a more precise linear description of the turbine while the respective flight envelope of the UH60. This was possible due to the fact that the pressure dependency of the turbo shaft model. For that reason, several characteristic curves were plotted and the euclidean distance within the operation space was determined. The reference pressure is chosen as the ambient pressure p_{amb}. Furthermore,

$$\tilde{\beta}_0 = C_p(1 - \frac{p}{p_{amb}}) + \beta_0 \tag{2.4}$$

with $C_p = 219\frac{s}{min}$ is formulated for simplification purposes which serves as an adapted version of the constant term.

2.2.2 Modeling of the Transmission/Variator

The Variator

In order to realize the variable rotational speed of the rotor, a power split gearbox has to be built-in which consists of set of planetary gears and a drive-train [8]. The drive-train, provided by the power turbine, is divided into a mechanical path and a variator path [21] which has to allow gear ratios between zero and infinity and is a key component of the VARISPEED project.
The variator is a combination of a generator and a motor [22]. Depending on the demand of the rotor-craft, the variator will either supply power or safe excess power. Due to the inert nature of the power turbine, the variator has to compensate the energy demand in transient states of the helicopter.
For simplification purposes in regards of modelling, the variator was originally conceived to be mathematically represented by a constraint in the latter presented optimal controller. Yet, the motor generators play a coherent substitution role in the latter presented analogous model.

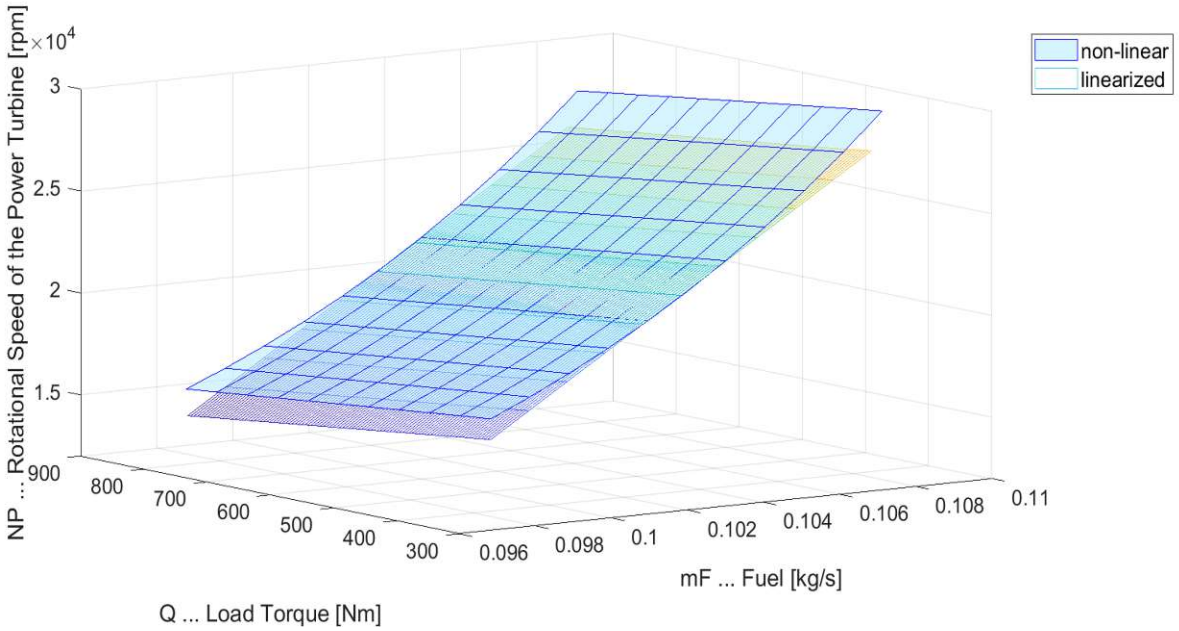

Figure 2.6: Characteristic Curve of the GE T700

The Transmission

A continuous-variable transmission system with a high degree of efficiency is only achieved by splitting the input power into a mechanical path and a variation path, as previously described, to allow the rotational speed to vary. This is done by using planetary gears which have two degrees of freedom. The rotational speed of each shaft can be varied independently [10].
Such power split transmission have at least one mechanical point for which the total power is transmitted by only the mechanical path. Transmission rations beyond the mechanical paths lead to a power flow in the variator path which leads to a decreased efficiency factor. There are three possible configurations of this kind of power split transmission - output split transmission, input split transmission and compound split transmission [23].
The compound split transmission is a combination of input split and output split. Fig. 2.7 illustrates a technical sketch of this configuration and its operation principle. It has two mechanical paths due to its two planetary gears where there is no power flow through the variator path. Between these mechanical points, one variator works as a generator and the other works a motor [23, 8].

In the further technical integration, two possible drive-train architectures are conceivable. Due to the higher degree of difficulty in regards of implementation of architecture

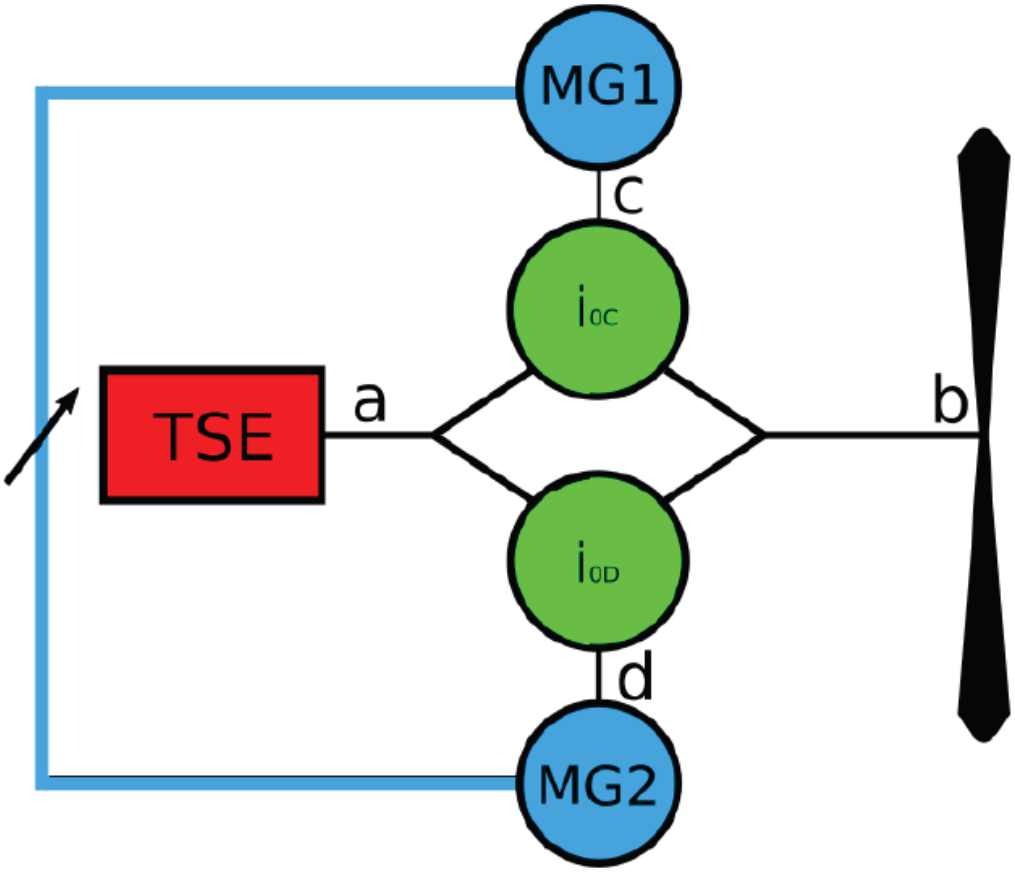

Figure 2.7: Compound Split Drive-Train: two epicyclic gear sets are positively connected to two shafts. Due to a lack of an energy storage device, the energy being introduced at MG 1 is equal to the one in MG 2. The mechanical points constitute a boundary for the operation range of this device. The shaft linkage a and b determine the kinematic degree of freedom of two. [23]

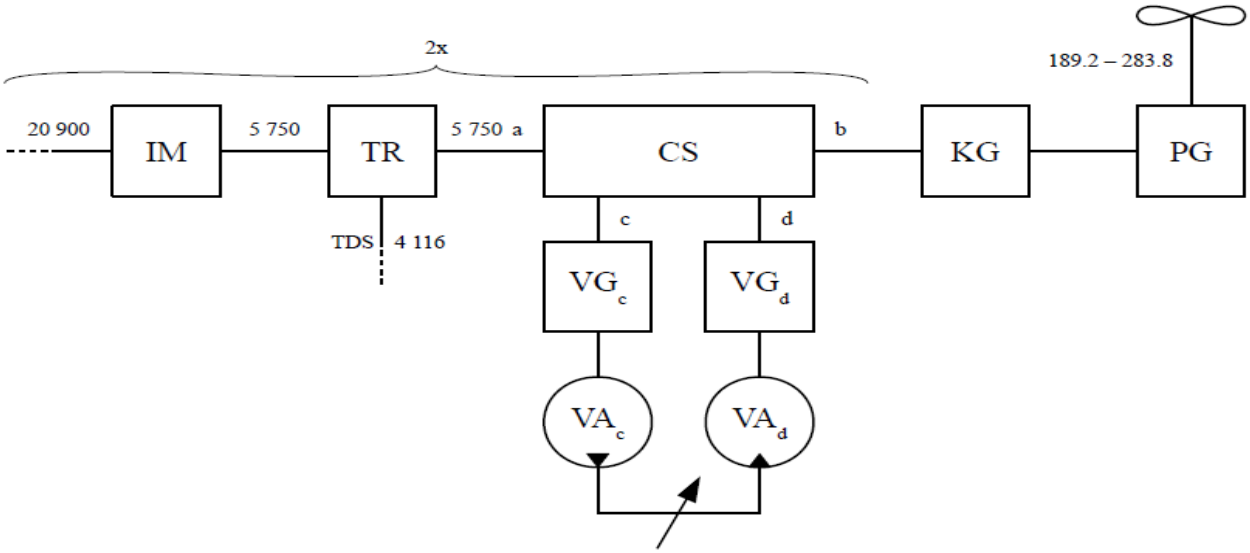

Figure 2.8: Architecture of the drive-train: the superior configuration in terms of allocation in space. The dual arrangement of the compound split before the bevel gear and the planetary gear set is a characteristic feature of this architecture [22].

one, architecture two could assert itself. Fig. 2.8 shows architecture two. It is characterized by the position of the two compound splits which are located before the bevel gear and the planetary gear set. An additional benefit of architecture two was that the tail rotor was not effected by the variation of the rotational speed [22].

2.3 The Analogous Model

Regarding the adherence to the principle of similarity in terms of modelling, an analogous model was introduced. The Hybrid Synergy Drive (HSD) was an eligible choice to fill this role which was taken as a complete model from [24]. The drive-train, a combustion engine, two motor generators, MG 1 and MG 2, and a planetary gear, resemble the configuration of the original system, sufficiently. A non-linear spring-damper element with a rotational mass being attached to it serves as a dynamical representation of rotor model. Yet, no direct inputs of the driver are considered in this model. Figure 2.9 illustrates the composition of this hybrid drive-train.

Within this configuration the following must be considered: An electronic controller

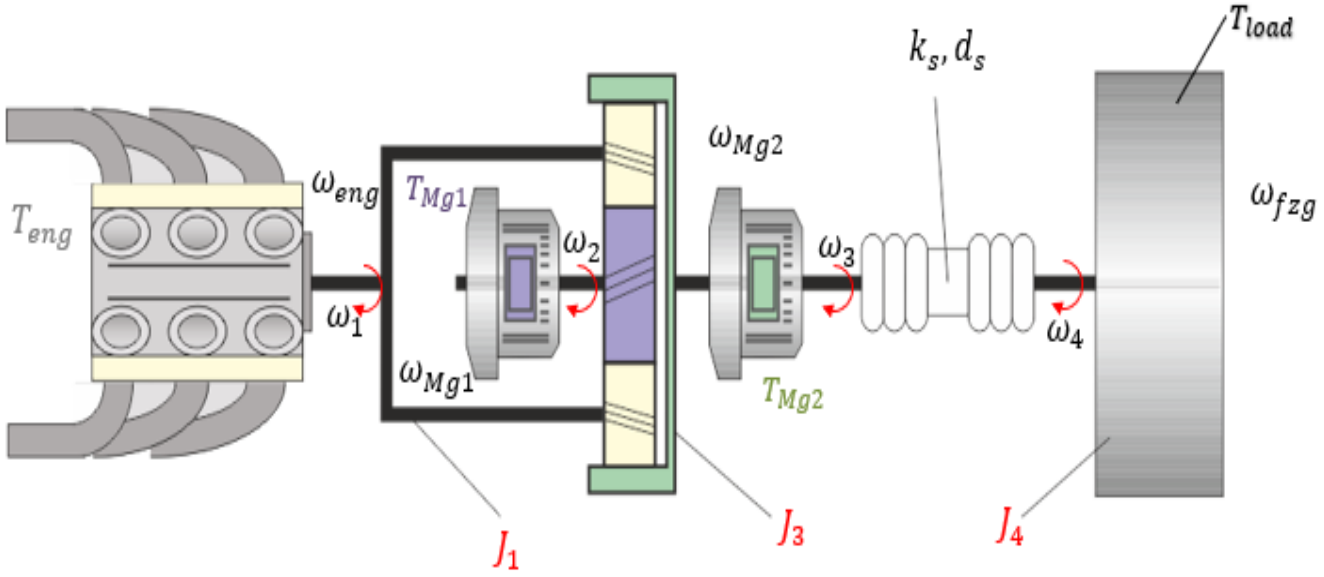

Figure 2.9: Hybrid Synergy Drive (HSD): A combustion engine is over a planetary gear linked to two motor generators, MG1 and MG2. MG1, the smaller motor generator, is connected to the sun wheel. The planetary gears are linked with the shaft of the internal combustion. The larger motor generator, MG2, is connected to the outer gear rim. A reduced rotational mass is adjusted via a spring-damper element to MG2.

regulates the transmission ratio between the combustion engine and the output shaft. The motor generator can either function as a motor or a generator. The power flow between inside the planetary gear is dependent to the constituted power distribution of the combustion engine and the two motor generators.
The Hybrid Synergy Drive manages without a coupling. Every component of it is positively connected with each other which allows for the full operation range of the combustion engine from standstill to maximum speed.
An additional starter is not required. The motor generators are controlled in such a way that they provide an ejection torque for the combustion engine. Furthermore, a mechanical reverse gear is not necessary. MG2 carries over this function. The following operation states of the drive-train exist:

1. Purely electric start-up: the battery provides electrical power
2. Load point increase: the combustion engine drives the vehicle while the motor generator charges the battery
3. Both, combustion engine and motor generator, drive the vehicle while the other motor generator provides the required electrical energy
4. Load point reduction: the combustion engine and the motor generator drive the vehicle while the battery supplies the required electrical energy
5. Sailing: while allow rolling the combustion engine is off, the motor generator carries out a light pre-breaking, braking energy is utilised to charge the battery
6. Regenerative braking: braking energy is used for charging the battery, braking is performed by the motor generator and the mechanical brake

In order to ensure a reasonable efficiency factor, an operation range of 1000 rpm − 4500 rpm has to be maintained for the rotational speed of the combustion engine. This needs to be taken into account in the control design.
A more detailed description about the structure, varieties and application hybrid drive-train systems can be found in [25]. In [26] an investigation of such hybrid drive-trains was carried out.

Chapter 3

Theoretical Background

3.1 Local Linear Model Network

The Local liner model network is a potent method to deal with the control of non-linear system[27]. It has superior features in comparison with neural network such as a reduced curse of dimensionality and transparency [28]. One issue with local linear models is that the model is usually only valid closely around the equilibrium point [29] and meaningful interpolation between the models is a challenging task [27]. Given a non-linear system

$$\boldsymbol{x}(k+1) = \boldsymbol{f}(\boldsymbol{x}(k), \boldsymbol{u}(k)) \tag{3.1}$$

$$\boldsymbol{y}(k) = \boldsymbol{h}(\boldsymbol{x}(k)) \tag{3.2}$$

[30] for which a multiple model network shall be designed. Such a local linear model network (for a first-order system) is represented the following way

$$\hat{y}(k+1) = \sum_{i=1}^{n} \phi_i(k) M_i(k) \tag{3.3}$$

where $\hat{y}(k+1)$ is prediction of the output in the next time step, $\phi_i(k)$ represents the i-th validity function or membership function and $M_i(k)$ is the i-th local model output [31]. In figure 3.1, the local linear model network of a first-order system is visualized which is located in the $u(k) - y(k) - y(k+1)$ space and is limited by the operating space $\mathbb{R}^2 \sqsubseteq u(k) - y(k)$ space. Its partitioning can be conducted by a metric like equidistant points or the ν gap metric, which will be introduced later, or expert knowledge. Each operating point determines the location of a local linear model. The structure of the validity function and the type of local model play a crucial role in the design of a multiple model network [32].

Within the domain of local linear model networks, there are several ways of development. For local linear model, mathematical models are used [32] which can be divided

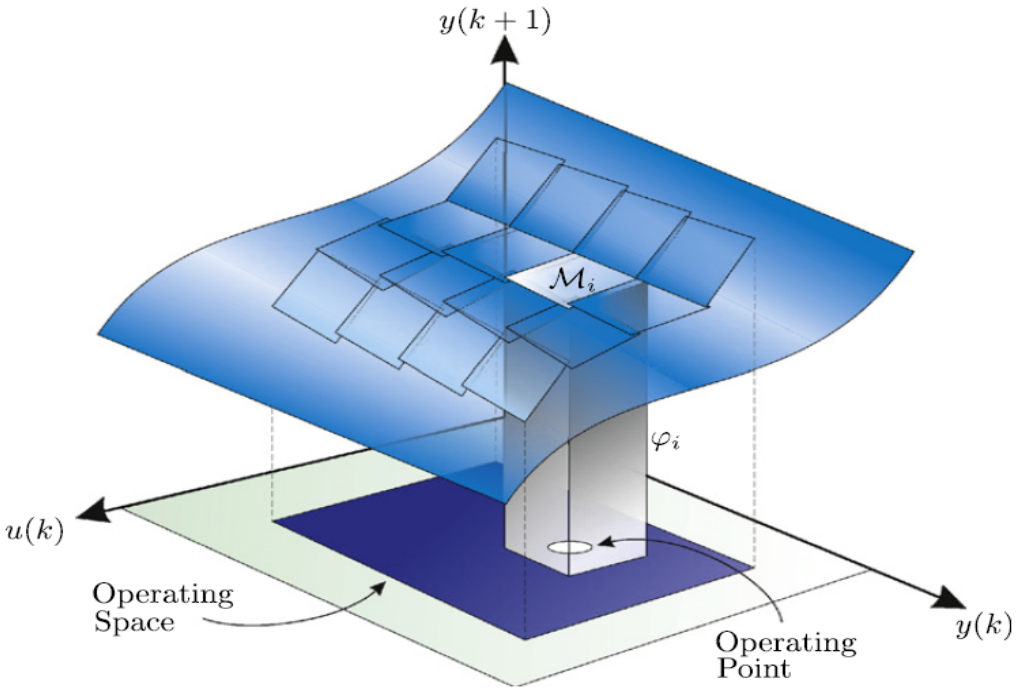

Figure 3.1: Illustration of a local linear model network structure[32]

into analytic models which are derivations of mathematical formulations of the laws of physics and experimental models [33] which are based on empirical data. The simplest form of analytical model can be solely a weight [32].
In order to receive a linear local model, one must either linearize an analytic model in its respective operating points or determine the model structure from experimental data through parameterizing by black-box modeling [34, 33]. By applying black-box model structures, one is able to accommodate a model structure without referring to its internal structure. Some of its prominent representatives are ARMAX, ARX, Box-Jenkins and Output Error model etc. [35].
Additionally, a structure of validity functions has to be chosen. Radial basis functions networks or Takagi-Sugeno fuzzy models are possible candidates. The validity functions allocate to each local linear model its respective validity space and has a value of one at its respective operating point. In order to keep unity, validity function have to be normalised. This implies that at least one model will always be active. Unfortunately, unwanted side effects of this method are the necessary evil to bear [32].
A key aspect of designing a local model network is structure optimisation to ensure an optimal number of local models, their position, the shape of the validity function and a suitable scheduling vector [32] to describe the most pronounced non-linearities of

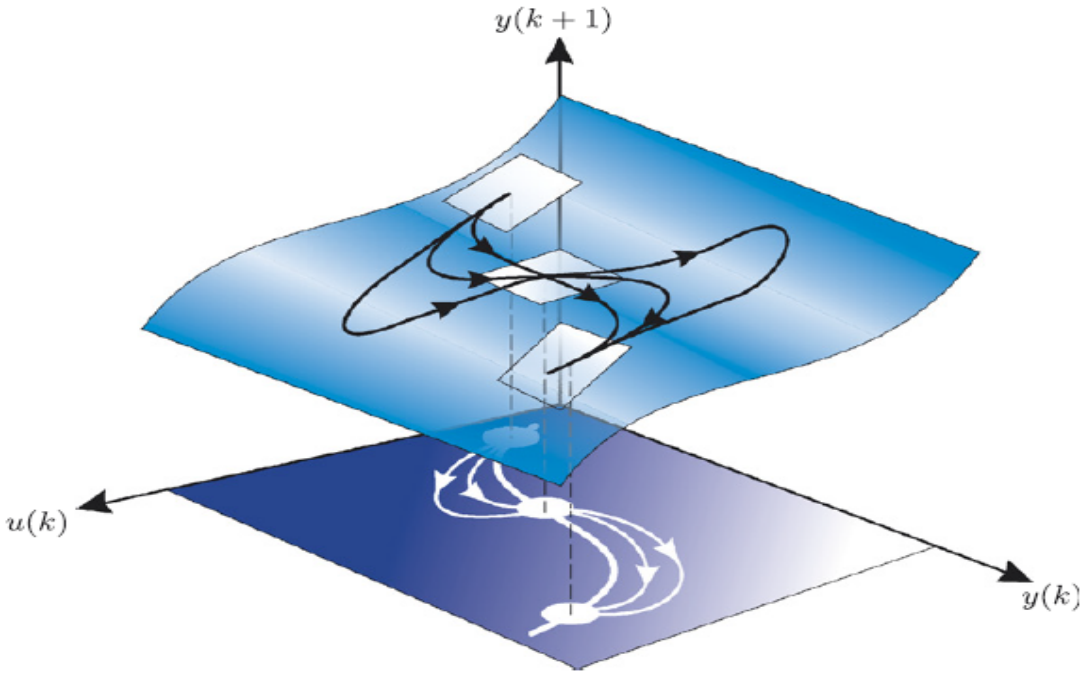

Figure 3.2: The off-equilibrium problem [32]

the given process [36]. The two opposing methods - forward and backward regression - come to the fore. In case of forward regression, an initially simple model structure is assumed which is gradually increased until it fits the complexity of the system [37]. Backward regression, on the other hand, presumes a complex structure which is being simplified until the required fit is achieved [38].
Off-equilibrium dynamics are an essential problem of multiple model networks. They occur when the system moves far away from the equilibrium points where the system is extrapolated [39]. Those effects are less pronounced when the value of the entries of the scheduling vector change more moderately. Fig. 3.2 illustrates this phenomena with local linear model network consisting of three models of non-linear function of first-order. Too aggressive system behavior maneuvers the system into undefined regions which causes detrimental off-equilibrium dynamics [32]. An effective solution of this problem is the velocity linearization approach [40] which is not further discussed here.

Finally, after having created a template for the local linear model network, the local models have to be interpolated. This can be done by two ways - output blending or parameter blending [41, 42].

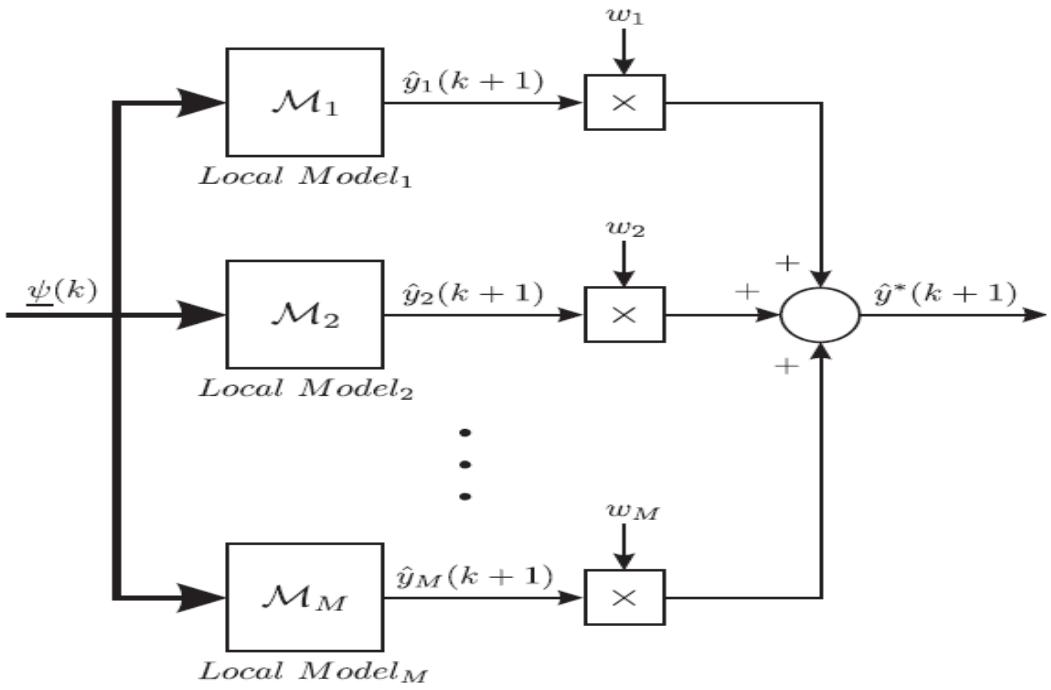

Figure 3.3: Output blending of a linear local model network[32]

Output blending interpolates between the outputs of each output model regarding their current validity, respectively. This is mathematically modelled by a weighted sum

$$\hat{y}(k+1) = \sum_{i=1}^{n} w_i \hat{y}_i(k+1) \tag{3.4}$$

where $\hat{y}(k+1)$ is the output of the multiple model in the next time step, w_i is the validity function and $\hat{y}_i(k+1)$ is the output of the individual model in the next time step [32]. A promising advantage of this approach is that different types of models can be combined to create a hybrid model like black-box models and and first-principle models, in order to overcome problematic system behaviour [43]. Fig. 3.3 illustrates this issue by the example of blending m local models by the output.

The other opposing approach is parameter blending which requires necessarily a common structure among all the models. The overall model output of the multiple model network is a linear combination of the parameters of the local models

$$\hat{y}(k+1) = \underline{\psi}(k)^T \sum_{i=1}^{n} w_i \underline{\theta}_i \tag{3.5}$$

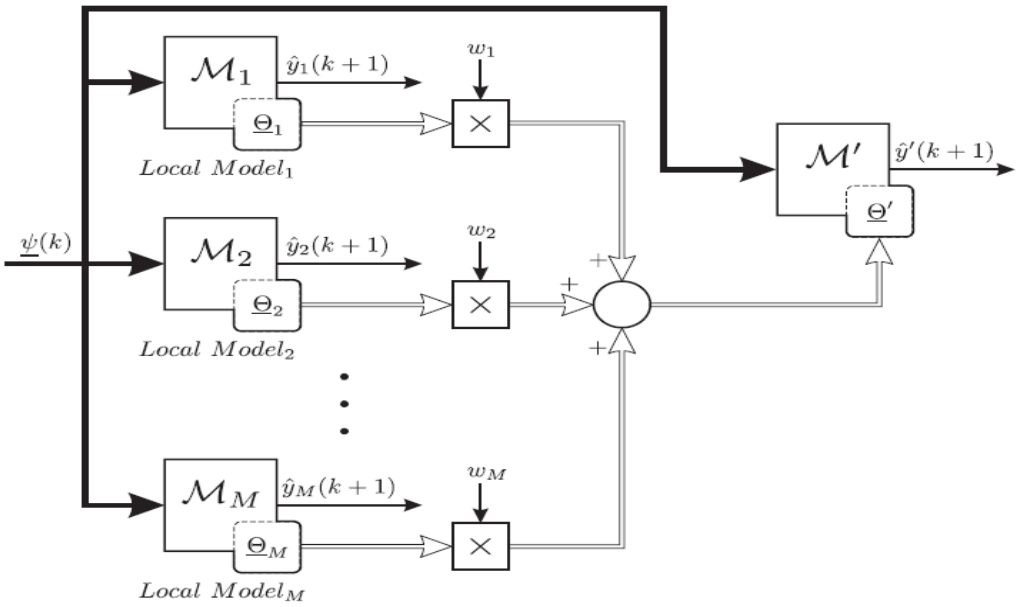

Figure 3.4: Parameter blending of a linear local model network[32]

where $\hat{y}(k+1)$ denotes the output of the multiple model in the next time step, w_i is the validity function and $\underline{\psi}(k)$ is the model structure and $\underline{\theta}_i$ are the parameters of the participating models [32]. Fig. 3.4 depicts again a multiple model network of m models being parameter blended.

3.2 Partition by the ν Gap Metric

The ν gap metric is one possible way of partitioning the operation space of a non-linear system which has gained more and more attention in the previous years [44, 45]. This method evaluates the distance between to operating points from the controller point of view by the H_∞ norm [44].

Let

$$P = NM^{-1} \tag{3.6}$$

be the normalized coprime factorization of a transfer function [46, 45] where N and M must satisfy the condition

$$\tilde{M}M + \tilde{N}N = I \tag{3.7}$$

where $(\sim)$ denotes the complex conjugate [45]. The graph of P is a subspace of the Hardy space and is given by

$$G(P) = \begin{bmatrix} M \\ N \end{bmatrix} H_2 \tag{3.8}$$

.

The ν gap between two finite-dimensional linear systems P_1 and P_2 of the same size in respect to input and output is given by [47]

$$\delta(P_1, P_2) = \|\Pi_{G(P_1)} - \Pi_{G(P_2)}\| \tag{3.9}$$

where Π is the orthogonal projection. The ν gap between the systems P_1 and P_2 can be computed by

$$\delta(P_1, P_2) = max\{\overrightarrow{\delta}(P_1, P_2), \overrightarrow{\delta}(P_2, P_1)\} \tag{3.10}$$

where $\overrightarrow{\delta}(P_1, P_2)$ denotes the directed ν gap which can be determined by [48]

$$\overrightarrow{\delta}(P_1, P_2) = \inf_{Q_1 \in H_\infty} \| \begin{bmatrix} M_1 \\ N_1 \end{bmatrix} - \begin{bmatrix} M_2 \\ N_2 \end{bmatrix} Q_1 \|_\infty \tag{3.11}$$

.

H_∞ is the Hardy space with the norm [48]

$$\|\Delta(s)\|_\infty = max_\omega\{\Delta(j\omega)\} \tag{3.12}$$

where $\tilde{\sigma}(.)$ denotes the maximum singular value of $\Delta(j\omega)$ and Q_1 is any function that is a subspace of H_∞ [48]. The boundaries for the ν is

$$0 \leq \delta(P_1, P_2) \leq 1 \tag{3.13}$$

.

by definition. Value of $\delta(P_1, P_2)$ on the lower bound indicate that the distance between both investigated systems is small within the H_∞ space, whereas, on the contrary, the upper bound suggest significantly different dynamical behaviour. This means if the distance is small, there will be a controller which can stabilize both systems [46]. In order to ensure that generalized stability margin for a threshold value of the ν gap

$$\delta(P_1, P_2) \leq \epsilon \tag{3.14}$$

must hold [44].

3.3 Fuzzy Logic and Fuzzy Controller

3.3.1 Fuzzy Logic

Classical mathematical approaches are based on the assumption that formal propositions can be always assigned in an binary manner as true or false [49]. This applies for a wide scope of problem settings within mathematics. A different approach aims to capitalize the vagueness of colloquial speech for control engineering purposes. In order to achieve that expressions like "slightly big", "moderately small" e.g. have be conceptualizable for a machine. Those vague concepts might be suitable for human interaction without any problem but create huge difficulties to process for a machine with usual mathematical tools [50].

Fuzzy logic solves that problem by discarding the discrete distinction of a given element. Rather, gradual differences of elements are implemented in a mixed mathematical framework of discrete elements with continuous transitions between them [50]. To each of those elements a membership function is associated which describes the degree of belonging to a certain set [35].

Definition 1 *A fuzzy set μ is a class of elements X with the function $\mu : X \to [0, 1]$ which assigns each value $x \in X$ its degree of membership $\mu(x)$ to μ [51, 52].*

The interpretation of the membership to a fuzzy set can be difficult to grasp. While a value of one, denotes an absolute membership to one particular set, a distinction between values of 0.7 and 0.8 loses their distinctness [50].
As for classical sets, fuzzy logic applies a distinct range of operations which are the following [49, 53, 54]:

1. fuzzy intersection (AND)
2. fuzzy union (OR)
3. fuzzy complement (NOT)

The logical AND can be specified as a binary mapping T of two given membership function. Two possible T-norm operators for fuzzy intersection are minimum

$$T_{min}(\mu_A(x), \mu_B(x)) = min(\mu_A(x), \mu_B(x)) \tag{3.15}$$

and the algebraic product

$$T_{ap}(\mu_A(x), \mu_B(x)) = \mu_A(x)\mu_B(x). \tag{3.16}$$

For the logical OR, the binary mapping S of two membership functions is defined. The S-norm for the fuzzy union can be realized as a maximum

$$S_{max}(\mu_A(x), \mu_B(x)) = max(\mu_A(x), \mu_B(x)) \tag{3.17}$$

and the algebraic sum

$$S_{ap}(\mu_A(x), \mu_B(x)) = \mu_A(x) + \mu_B(x) - \mu_A(x)\mu_B(x). \tag{3.18}$$

The fuzzy NOT is of a membership function is mathematically defined as

$$\mu_{\bar{A}}(x) = 1 - \mu_A(x). \tag{3.19}$$

3.3.2 Fuzzy Controller

Three main aspects that fuzzy controllers differ from other control techniques are [55]

1. if-then rules
2. general approximation property and
3. the power to cope with set-wise inputs.

In order to express the plants behaviour, fuzzy rules have to be identified which mimic the plants response sufficiently well and fulfill the control objectives. Either knowledge acquisition or black box modeling can be used to establish proper if-then rules for the fuzzy controller [55].
Referring to the second feature of a fuzzy control technique, any continuous function on a compact set can be approximated by a fuzzy system. This is done with a finite number of fuzzy sets and corresponding membership functions [55].
The third characteristic of fuzzy controllers as mentioned above, is the capability to deal with fuzzy values in vague terms rather than crisp values [55].

For a fuzzy controller, a fuzzy inference system is defined which consists of four components fuzzy rule base, fuzzification, fuzzy inference and defuzzification. Fig. 3.5 serves as an illustration of the fuzzy inference principle [49].

Fuzzy rule base, the foundation of a whole fuzzy inference, is a set of a defined amount of "IF-THEN" rules [49]. The IF part, or antecedent of a rule, and the THEN part, the consequent part of the rule, constitute the fuzzy inference which is mathematically formulated as the following [56]

$$\text{IF an antecedent proposition THEN a consequent proposition} \tag{3.20}$$

The consequent proposition can be subdivided into three forms:

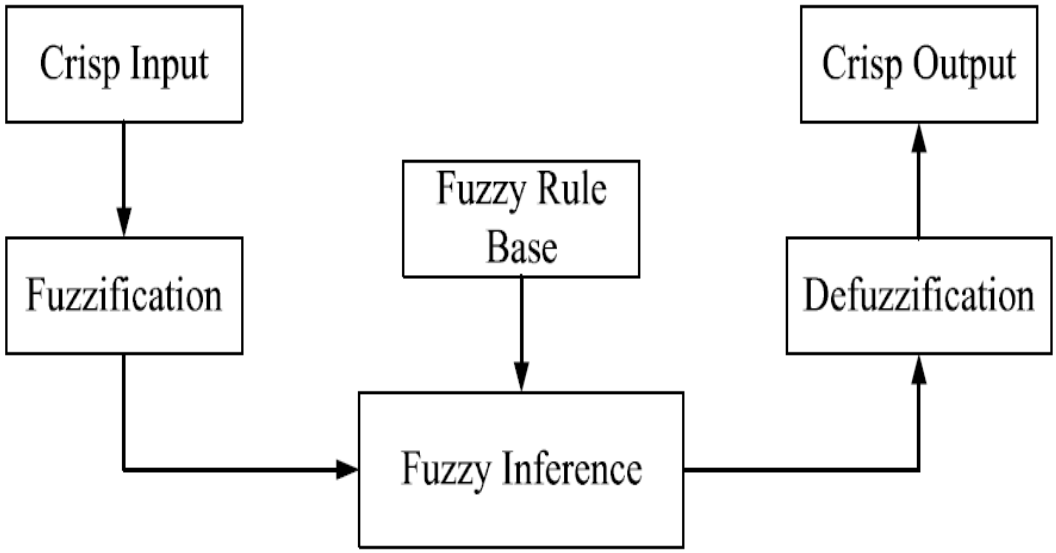

Figure 3.5: Fuzzy inference system[49]

1. Crisp consequent:

$$\text{IF an antecedent proposition THEN } y = y_a \tag{3.21}$$

2. Fuzzy consequent:

$$\text{IF an antecedent proposition THEN } y = Y_k \tag{3.22}$$

3. Functional consequent:

$$\text{IF } z_1 \in A_1 \wedge ... \wedge z_m \in A_m \text{ THEN } y = f(z_1, ..., z_m) \tag{3.23}$$

The fuzzification merges the crisp values z_i with each other to create fuzzy variables [49]. Therefore, a series of membership function can be used like triangular, trapezoidal, Gaussian's and more [55].
For defuzzification, or in other words fuzzy-to crisp-conversion, again a series of methods can be applied like maximum defuzzification, center of gravity defuzzification, center average defuzzification and others [49].

3.3.3 Takagi-Sugeno Fuzzy Model

Mamdani fuzzy systems and Takagi-Sugeno fuzzy systems are considered prominent control techniques within the realm of fuzzy systems. Both differ by the consequent rule in the defuzzification phase from each other [49]. In Takagi-Sugeno fuzzy systems, a functional proposition is characteristic [57]. Also, for both, continuous and discrete time systems, Takagi-Sugeno fuzzy models can be applied [58].
The general inference of a Takagi-Sugeno fuzzy system looks like the following [49, 56]

$$R^i\text{: IF } z_1 \in A_1^i \wedge ... \wedge z_m \in A_m^i \text{ THEN } y = f_i(z_1, ..., z_m) \tag{3.24}$$

where R^i denotes the i-th fuzzy rule, $z_1, ..., z_m$ are input variables, f_i denotes a crisp function and A_m^i are fuzzy sets linked to a respective membership function $\mu_{A_m}^i(x_m)$ where $i = 1, ..., n$ and $j = 1, ..., m$.
For the fuzzification method, trapezoidal, triangular, Gaussian, singleton etc. can be used. Additionally, for a multiple fuzzy sets the product operator connects the individual fuzzy variables in the fuzzification phase which takes the form of

$$\lambda_i(z) = \prod_{j=1}^{m} \mu_{A_m^i}(z_j) \tag{3.25}$$

with $z = [z_1, z_2, ..., z_m]^T$.
For the defuzzification, the weighted average method is used over all the local models:

$$y = \frac{\sum_{i=1}^{n} \lambda_i(z) f_i(z)}{\sum_{i=1}^{n} \lambda_i(z)} \tag{3.26}$$

which can be further simplified to

$$y = \sum_{i=1}^{n} \mu_i(z) f_i(z) \tag{3.27}$$

where $\mu_i(z)$ is normalized firing strength

$$\mu_i(x) = \frac{\lambda_i(z)}{\sum_{i=1}^{n} \lambda_i(z)} \tag{3.28}$$

3.3.4 Takagi-Sugeno Model-Based Fuzzy System

Takagi-Sugeno fuzzy systems are adequate to be combined with model-based control approaches[59, 52]. For model-based control techniques, the following control scheme

$$\boldsymbol{u}(t) = \boldsymbol{K}x(t) \tag{3.29}$$

is primarily used [60]. Together with 3.24 a control law

$$R^i\text{: IF } z_1 \in A_1^i \wedge ... \wedge z_m \in A_m^i \text{ THEN } \boldsymbol{u}_i = \boldsymbol{K}_i \boldsymbol{x}(t) \tag{3.30}$$

for TS model-based fuzzy systems is obtained where $i = 1, ..., n$ [60].

3.4 Model Predictive Control

Model Predictive Control (MPC) is not a specific control technique but rather a loose term specifying an ample range of control methods which have in common the minimization of an objective function. These control designs share a mutual foundation but differ in certain features [61, 62]. Generalized Predictive Control (GPC), Dynamic Matrix Control (DMC) and Model Algorithmic Control (MAC) are some prominent examples of its wide range [62]. The connecting basis of all members of the predictive control family share the following properties [61, 63, 62]:

1. Explicit exploitation of the determinism of the underlying model structure enables a future output prediction at a future horizon .
2. Computation of a control sequence by optimizing plant behavior.
3. A receding horizon principle which is moves forward towards the future after each time instant, applying only the first control signal of the sequence and discarding the residuals .

Next to its natural handling of multi-variable control problems, its well suitable structure for online optimizations and consideration of actuator limitations, it allows due to its possibility of setting constraints to manage to adapt to rough environmental conditions of the process industry [64, 63]. The following section will dive more into detail about the foundation of Model Predictive Control and its mathematical formulation for state space models.

3.4.1 State Space Formulation

Model predictive control uses the mathematically modelled dynamical structure together with disturbances and constraints, the current and future outputs and the future control inputs and the given trajectory to compute the optimal model output which minimizes the difference between the output prediction and the reference trajectory. The number of future control outputs and control inputs taken into account are determined by the prediction horizon N_c and the control horizon N_u [56] which play

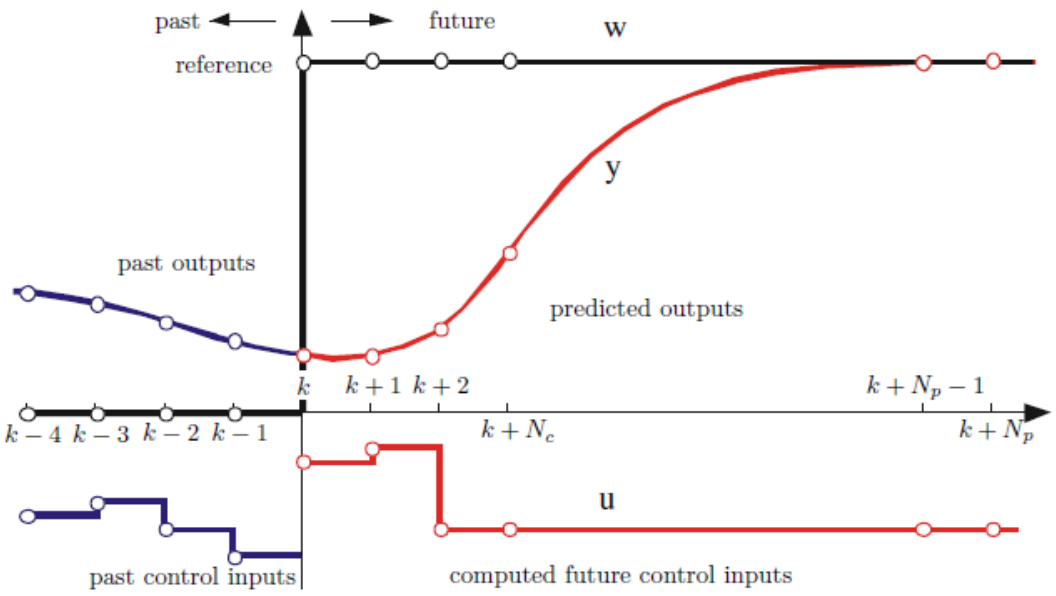

Figure 3.6: Fundamental Principle of Model Predictive Control[62]

fundamental roles in the MPC design. Fig. 3.6 illustrates this principle.

The foundation of the model predictive control algorithm is mathematically speaking an optimization problem for which the cost function in a quadratic form

$$J = (\boldsymbol{Y}_{ref} - \boldsymbol{Y})^T(\boldsymbol{Y}_{ref} - \boldsymbol{Y}) + \boldsymbol{\Delta U}^T \boldsymbol{R} \boldsymbol{\Delta U} \tag{3.31}$$

is set up to predicatively respond to the set point signal [65]. The quadratic cost function is minimized

$$\min_{\boldsymbol{\Delta U}(k)} J \tag{3.32}$$

with each time step with respect to $\boldsymbol{\Delta U}(k)$. Here, a model-based predictive controller for a state space system will be contemplated. Consider

$$\boldsymbol{x}_m(k+1) = \boldsymbol{A}\boldsymbol{x}_m(k) + \boldsymbol{B}\boldsymbol{u}(k) + \boldsymbol{E}\boldsymbol{z}(k) \tag{3.33}$$

$$\boldsymbol{y}(k) = \boldsymbol{C}\boldsymbol{x}_m(k) \tag{3.34}$$

which denotes a classical state space formulation in MIMO format where $\boldsymbol{u}(k)$, $\boldsymbol{x}_m(k)$, $\boldsymbol{y}(k)$ and $\boldsymbol{z}(k)$ are the input vector, the state vector, the output vector and the vector of measurable disturbances, respectively. $\boldsymbol{A}$, $\boldsymbol{B}$, $\boldsymbol{C}$ and $\boldsymbol{E}$ are the system matrix, the

input matrix, the output matrix and the disturbance matrix, respectively. Here, a key advantage of model-based predictive control is observable which is that there is no distinction between SISO and MIMO cases. Rather the SISO configurations can be contemplated as a special case.
Now, the discrete time state space equations are reformulated to embed an integrator into the state space system which guarantees high tracking performance [62]. The following steps are based on [66]. The state space variables are incremented in the following way

$$\Delta \boldsymbol{x}_m(k+1) = \boldsymbol{A}\Delta \boldsymbol{x}_m(k) + \boldsymbol{B}\Delta \boldsymbol{u}(k) + \boldsymbol{E}\Delta \boldsymbol{z}(k) \tag{3.35}$$

such that the control variable $\boldsymbol{x}_m(k+1)$ is denoted by

$$\boldsymbol{\Delta x}_m(k+1) = \boldsymbol{\Delta x}_m(k+1) - \boldsymbol{\Delta x}_m(k)$$

and that the same applies for the input vector $\boldsymbol{u}(k)$

$$\boldsymbol{\Delta u}(k) = \boldsymbol{u}(k) - \boldsymbol{u}(k-1)$$

and the vector of measurable disturbances $\boldsymbol{z}(k)$

$$\boldsymbol{\Delta z}(k) = \boldsymbol{z}(k) - \boldsymbol{z}(k-1).$$

A new state vector is defined by

$$\boldsymbol{x}(k) = \left[\boldsymbol{\Delta x}_m(k)^T y(k)\right]^T \tag{3.36}$$

which is commonly labeled as the augmented state vector. By inserting 3.35 in 3.36 and defining a new output matrix, one receives

$$\begin{bmatrix}\boldsymbol{\Delta x}_m(k+1)\\ \boldsymbol{y}(k+1)\end{bmatrix} = \begin{bmatrix}\boldsymbol{A}_m & \boldsymbol{0}_m^T\\ \boldsymbol{C}_m\boldsymbol{A}_m & \boldsymbol{I}\end{bmatrix}\begin{bmatrix}\boldsymbol{\Delta x}_m(k)\\ \boldsymbol{y}(k)\end{bmatrix} + \begin{bmatrix}\boldsymbol{B}_m\\ \boldsymbol{C}_m\boldsymbol{B}_m\end{bmatrix}\boldsymbol{\Delta u}(k) + \begin{bmatrix}\boldsymbol{E}\\ \boldsymbol{C}_m\boldsymbol{E}\end{bmatrix}\boldsymbol{\Delta z}(k) \tag{3.37}$$

$$\boldsymbol{y}(k) = \begin{bmatrix}\boldsymbol{0} & \boldsymbol{I}\end{bmatrix}\begin{bmatrix}\boldsymbol{\Delta x}_m(k+1)\\ \boldsymbol{y}(k+1)\end{bmatrix} \tag{3.38}$$

where $\boldsymbol{0}_m$ and $\boldsymbol{I}$ denote a zero matrix and an identity matrix with suitable dimensions, respectively. The augmented state space equations of the model predictive controller can be reformulated in the following way

$$\boldsymbol{x}(k+1) = \boldsymbol{A}\boldsymbol{x}(k) + \boldsymbol{B}\boldsymbol{\Delta u}(k) + \boldsymbol{E}\boldsymbol{\Delta z} \tag{3.39}$$

$$\boldsymbol{y}(k) = \boldsymbol{C}\boldsymbol{x}(k) \tag{3.40}$$

which allow a comfortable application of the framework. The characteristic polynomial [67]

$$P(k) = det \begin{bmatrix} \lambda \boldsymbol{I} - \boldsymbol{A}_m & \boldsymbol{0}_m^T \\ -\boldsymbol{C}_m \boldsymbol{A}_m & (\lambda - 1)\boldsymbol{I}_{n_y x n_y} \end{bmatrix} = (\lambda - 1)^{n_y} det(\lambda \boldsymbol{I} - \boldsymbol{A}_m) = 0 \tag{3.41}$$

demonstrates clearly the effects of the augmentation of the state space model. For each model output, an integrator is added to the model which prevents steady state errors.

Both the concepts controllability and observability play integral roles in the design of a model predictive controller. This is especially the case when dealing with unstable dynamics. Controllability is an essential requirement to ensure stability and observability is the foundation in observer design [66]. Nevertheless, stabilizability and detectability are the least requirements when the concern is only closed-loop stability. The definition of minimal realisation allows an eased way to determine whether a system is controllable and observable [68].

Theorem 1 *Minimal Realisation*
A realisation of a transfer function $\boldsymbol{G}(z)$ *is any state-space triplet* $(\boldsymbol{A}, \boldsymbol{B}, \boldsymbol{C})$ *such that* $\boldsymbol{G}(z) = \boldsymbol{C}(z\boldsymbol{I} - \boldsymbol{A})^{-1}\boldsymbol{B}$. *If such a set* $(\boldsymbol{A}, \boldsymbol{B}, \boldsymbol{C})$ *exists, then* $\boldsymbol{G}(z)$ *is said to be realisable. A realisation* $(\boldsymbol{A}, \boldsymbol{B}, \boldsymbol{C})$ *is called minimal realisation of a transfer function if no other realisation of smaller dimensions of the triplet exists [66].*

Again, the framework for model predictive control of [66] is used for the following part. In order to allow the controller to act predicatively, the stacked state space equation

$$\boldsymbol{Y} = \boldsymbol{F}\boldsymbol{x}(k) + \boldsymbol{\Phi}_u \boldsymbol{\Delta U} + \boldsymbol{\Phi}_z \boldsymbol{\Delta Z} \tag{3.42}$$

is formulated which exploits the deterministic and recursive nature of state space systems. Here, the stacked inputs and outputs are

$$\boldsymbol{Y} = \left[\boldsymbol{y}(k+1|k)^T \boldsymbol{y}(k+2|k)^T ... \boldsymbol{y}(k+N_p|k)^T\right]^T,$$

$$\boldsymbol{\Delta U} = \left[\boldsymbol{\Delta u}(k)^T \boldsymbol{\Delta u}(k+1)^T ... \boldsymbol{\Delta u}(k+N_c-1)^T\right]^T,$$

$$\boldsymbol{\Delta Z} = \left[\boldsymbol{\Delta z}(k)^T \boldsymbol{\Delta z}(k+1)^T ... \boldsymbol{\Delta z}(k+N_p-1)^T\right]^T$$

respectively with

$$\boldsymbol{F} = \begin{bmatrix} \boldsymbol{CA} \\ \boldsymbol{CA}^2 \\ \vdots \\ \boldsymbol{CA}_p^N \end{bmatrix}, \boldsymbol{\Phi} = \begin{bmatrix} \boldsymbol{CB} & \boldsymbol{0} & \boldsymbol{0} & \dots & \boldsymbol{0} \\ \boldsymbol{CAB} & \boldsymbol{CB} & \boldsymbol{0} & \dots & \boldsymbol{0} \\ \boldsymbol{CA}^2\boldsymbol{B} & \boldsymbol{CAB} & \boldsymbol{CB} & \dots & \boldsymbol{0} \\ \vdots & \vdots & \vdots & & \vdots \\ \boldsymbol{CA}^{N_p-1}\boldsymbol{B} & \boldsymbol{CA}^{N_p-2}\boldsymbol{B} & \boldsymbol{CA}^{N_p-3}\boldsymbol{B} & \dots & \boldsymbol{CA}^{N_p-N_c}\boldsymbol{B} \end{bmatrix}$$

capturing the stacked system equations. The set-point information

$$\boldsymbol{Y}_{ref} = \begin{bmatrix} \boldsymbol{w}(k+1|k)^T \boldsymbol{w}(k+2|k)^T \dots \boldsymbol{w}(k+N_p|k)^T \end{bmatrix}^T$$

is gathered along the prediction horizon N_p. Now, 3.42 is inserted into 3.31 which again is inserted into the optimization problem 3.32. This is evaluated to

$$\boldsymbol{\Delta U} = (\boldsymbol{\Phi}_u^T \boldsymbol{Q}_y \boldsymbol{\Phi}_u + \boldsymbol{R})^{-1} \boldsymbol{\Phi}_u^T \boldsymbol{Q}_y (\boldsymbol{Y}_{ref} - \boldsymbol{F}\boldsymbol{x}(k) - \boldsymbol{\Phi}_z \boldsymbol{\Delta Z}) \tag{3.43}$$

which yields the control law. Under the principle of receding horizon, the control law becomes

$$\boldsymbol{\Delta u}(k) = \begin{bmatrix} \boldsymbol{I} & \boldsymbol{0} & \dots & \boldsymbol{0} \end{bmatrix} \boldsymbol{\Delta U} \tag{3.44}$$

which only keeps the first input while discarding the residual ones [44]. Finally, the current input of the model-based predictive controller yields to

$$\boldsymbol{u}(k) = \boldsymbol{u}(k-1) + \boldsymbol{\Delta u}(k). \tag{3.45}$$

Under the assumption of a constant reference signal $\boldsymbol{Y}_{ref}$, the control law 3.44 can be reformulated to

$$\boldsymbol{\Delta u}(k) = -\boldsymbol{K}_{mpc}\boldsymbol{x}(k) + \boldsymbol{K}_y \boldsymbol{y}_{ref}(k) \tag{3.46}$$

with the constant gains $\boldsymbol{K}_{mpc}$ and $\boldsymbol{K}_y$ which allows a closed-loop formulation of the state space system 3.37

$$\boldsymbol{x}(k+1) = (\boldsymbol{A} - \boldsymbol{B}\boldsymbol{K}_{mpc})\boldsymbol{x}(k) + \boldsymbol{B}\boldsymbol{K}_y \boldsymbol{y}_{ref}(k). \tag{3.47}$$

Further information can be found in [69].

3.4.2 Constraints

Another crucial advantage over other control techniques is the ability of the MPC to take constraints into account. Three types of constraints can be identified regarding their locus of application: [62].

1. constraints on the increment of the input variable
2. constraints on the amplitude of the input variable
3. constraints on the output variable
   a) hard constraints
   b) soft constraints

Output constraints can be subdivided according to their strictness. This is due to the fact that hard output constraints can conflict with other constraints [66]. Mathematically formulated, one yields the following expression

$$\boldsymbol{\Delta u}^{min} \leq \boldsymbol{\Delta u}(k+i) \leq \boldsymbol{\Delta u}^{max},\ i = 0, ..., N_c - 1$$

$$\boldsymbol{u}^{min} \leq \boldsymbol{u}(k+i) \leq \boldsymbol{u}^{max},\ i = 0, ..., N_c - 1$$

$$\boldsymbol{y}^{min} \leq \boldsymbol{y}(k+j) \leq \boldsymbol{y}^{max},\ j = 0, ..., N_p$$

which can be rewritten to a vector notation

$$\boldsymbol{\Delta U}^{min} \leq \boldsymbol{\Delta U} \leq \boldsymbol{\Delta U}^{max}$$

$$\boldsymbol{U}^{min} \leq \boldsymbol{U} \leq \boldsymbol{U}^{max}$$

$$\boldsymbol{Y}^{min} \leq \boldsymbol{Y} \leq \boldsymbol{Y}^{max}.$$

In order to receive a compact notation, the constraints have to be reformulated. Firstly, the constraints on the increment of the control variable are expressed as lower inequalities

$$\begin{bmatrix} -\boldsymbol{I} \\ \boldsymbol{I} \end{bmatrix} \boldsymbol{\Delta U} \leq \begin{bmatrix} -\boldsymbol{\Delta U}^{max} \\ \boldsymbol{\Delta U}^{min} \end{bmatrix}. \tag{3.48}$$

In the next step, the constraints on the amplitude of the input variable reformulated to

$$\begin{bmatrix} \boldsymbol{u}(k) \\ \boldsymbol{u}(k+1) \\ \boldsymbol{u}(k+2) \\ \vdots \\ \boldsymbol{u}(k+N_c+1) \end{bmatrix} = \begin{bmatrix} \boldsymbol{I} \\ \boldsymbol{I} \\ \boldsymbol{I} \\ \vdots \\ \boldsymbol{I} \end{bmatrix} \boldsymbol{u}(k-1) + \begin{bmatrix} \boldsymbol{I} & \boldsymbol{0} & \boldsymbol{0} & \dots & \boldsymbol{0} \\ \boldsymbol{I} & \boldsymbol{I} & \boldsymbol{0} & \dots & \boldsymbol{0} \\ \boldsymbol{I} & \boldsymbol{I} & \boldsymbol{I} & \dots & \boldsymbol{0} \\ \dots & & & & \\ \boldsymbol{I} & \boldsymbol{I} & \dots & \boldsymbol{I} & \boldsymbol{I} \end{bmatrix} \begin{bmatrix} \boldsymbol{\Delta u}(k) \\ \boldsymbol{\Delta u}(k+1) \\ \boldsymbol{\Delta u}(k+2) \\ \vdots \\ \boldsymbol{\Delta u}(k+N_c-1) \end{bmatrix} \tag{3.49}$$

which can again be rewritten to

$$-(\boldsymbol{C}_1\boldsymbol{u}(k-1)+\boldsymbol{C}_2\boldsymbol{\Delta U}) \leq -\boldsymbol{U}^{min} \tag{3.50}$$

and

$$(\boldsymbol{C}_1\boldsymbol{u}(k-1)+\boldsymbol{C}_2\boldsymbol{\Delta U}) \leq -\boldsymbol{U}^{min}. \tag{3.51}$$

Finally, hard constraints on the output are considered and reformulated to

$$\boldsymbol{Y}^{min} \leq \boldsymbol{F}\boldsymbol{x}(k)+\boldsymbol{\Phi}\boldsymbol{\Delta U}+\boldsymbol{\Phi}_z\boldsymbol{\Delta Z} \leq \boldsymbol{Y}^{max} \tag{3.52}$$

which allows the briefer notation

$$\begin{bmatrix}\boldsymbol{M}_1\\ \boldsymbol{M}_2\\ \boldsymbol{M}_3\end{bmatrix}\boldsymbol{\Delta U} \leq \begin{bmatrix}\boldsymbol{N}_1\\ \boldsymbol{N}_2\\ \boldsymbol{N}_3\end{bmatrix} \tag{3.53}$$

where

$$\boldsymbol{M}_1 = \begin{bmatrix}-\boldsymbol{C}_2\\ \boldsymbol{C}_2\end{bmatrix},\ \boldsymbol{M}_2 = \begin{bmatrix}-\boldsymbol{I}\\ \boldsymbol{I}\end{bmatrix},\ \boldsymbol{M}_3 = \begin{bmatrix}-\boldsymbol{\Phi}_u\\ \boldsymbol{\Phi}_u\end{bmatrix}$$

$$\boldsymbol{N}_1 = \begin{bmatrix}-\boldsymbol{U}^{min}+\boldsymbol{C}_1\boldsymbol{u}(k-1)\\ -\boldsymbol{U}^{max}-\boldsymbol{C}_1\boldsymbol{u}(k-1)\end{bmatrix},\ \boldsymbol{N}_2 = \begin{bmatrix}-\boldsymbol{\Delta U}^{min}\\ \boldsymbol{\Delta U}^{max}\end{bmatrix},\ \boldsymbol{N}_3 = \begin{bmatrix}-\boldsymbol{Y}^{min}+\boldsymbol{F}\boldsymbol{x}(k)+\boldsymbol{\Phi}_z\boldsymbol{\Delta Z}\\ -\boldsymbol{Y}^{max}-\boldsymbol{F}\boldsymbol{x}(k)-\boldsymbol{\Phi}_z\boldsymbol{\Delta Z}\end{bmatrix}$$

Finally, one obtains the compact form of

$$\boldsymbol{M}\boldsymbol{\Delta U} \leq \boldsymbol{\gamma} \tag{3.54}$$

which represents an additive constant to the overall cost function 3.31 and is associated to it by Lagrange multipliers. This yields a convex optimization problem which takes the form of a problem of quadratic programming [56, 70].

3.4.3 Stability of Discrete Time Model Predictive Control

In this section, an overview over the techniques regarding MPC stability will be given without diving to deep into mathematical proofs. Anyhow, the following three elaborated methods have been enforced to guarantee stability [71, 72, 73]:

1. Terminal equality constraint
2. Terminal cost function
3. Terminal constraint set

Besides those three techniques also combinations of them exist like terminal set and terminal constraint set or quasi-finite-horizon where all four methods are combined [71, 56].

For the following part [56, 73, 74] is used as a reference. Terminal equality constraints is a relatively easy way to ensure stability of the model-based predictive algorithm, even in the non-linear case. It is based on the stability theorem of Lyuapunov. Given is a non-linear, discrete time system 3.1, 3.2 for which the following cost function

$$J(k) = \sum_{p=1}^{N} h(\boldsymbol{x}(k+p|k), \boldsymbol{u}(k+p-1|k)) \tag{3.55}$$

is defined and the following constraints

1. $\boldsymbol{u}(k+p-1|k) \in U$
2. $\boldsymbol{x}(k+p|k) \in X$
3. $\boldsymbol{x}(k+N|k) = 0$

are set and with $p = 1, ..., N-1$. The last constraint explicitly denotes the terminal constraint. The following assumptions are made

1. $(\boldsymbol{x}, \boldsymbol{u}) = (\mathbf{0}, \mathbf{0})$ is an equilibrium point
2. the prediction horizon and the control horizon ($N_p = N_c$) have the same length
3. $h(.,.) \geq 0$
4. $h(.,.) = 0$ only if $\boldsymbol{x} = \mathbf{0}$ and $\boldsymbol{u} = \mathbf{0}$

The optimal value of the cost function $\hat{J}(k)$ is chosen as a Lyapunov function candidate. Now, it can be shown that $\hat{J}(k) \geq \hat{J}(k+1)$ which qualifies $\hat{J}(k)$ as a Lyapunov function and therefore guarantees stability.
Some critical comment have to made at this point. This proof is only valid if there is a global minimum of the cost function after each optimization (which is naturally the case for linear models and quadratic cost functions). Additionally, the length of the prediction horizon N_p plays a crucial role. If the length is insufficiently short then aiming to the desired state is an impossible task.
Alternatively, a terminal cost term can be added to cost function 3.31 to convert it into an infinite horizon problem

$$J(k) = \sum_{i=1}^{N_c} \{\hat{\boldsymbol{y}}^T(k+p)\boldsymbol{Q}_y\hat{\boldsymbol{y}}(k+p) + \boldsymbol{\Delta u}^T(k+i-1)\boldsymbol{R}\boldsymbol{\Delta u}(k+i-1)\} + \\ + \sum_{i=N_c+1}^{\infty} \hat{\boldsymbol{y}}^T(k+p)\boldsymbol{Q}_y\hat{\boldsymbol{y}}(k+p) \tag{3.56}$$

for which $\boldsymbol{\Delta u}^T(k+i-1) = 0$ for $i > N_c$. Now, 3.56 can be reformulated to

$$J(k) = \sum_{i=1}^{N_c} \{\hat{\boldsymbol{y}}^T(k+i)\boldsymbol{Q}_y\hat{\boldsymbol{y}}(k+i) + \boldsymbol{\Delta u}^T(k+i-1)\boldsymbol{R}\boldsymbol{\Delta u}(k+i-1)\} + \\ + \hat{x}^T(k+N_c)\boldsymbol{Q}\hat{\boldsymbol{x}}(k+N_c) \tag{3.57}$$

for which $\boldsymbol{Q}$ qualifies as a Lyapunov function and stability can be shown. The new form represents an ordinary control problem with an additional penalty term.

Here, additionally reference is made to [75, 76, 77]. For the third method, a set of admissible terminal states instead of a terminal state is used which are located in a certain neighborhood of the equilibrium points of the plant. The algorithm goes the following way: Initially, the predictive algorithm leads within a finite horizon the system states to the set of admissible terminal states, in a finite number of steps. Then, the controller is switched to a linear state feedback mode which brings the states to their respective equilibrium points. Due to its nature, this method is called dual-mode algorithm.

3.5 Fuzzy Model Predictive Control for State Space Systems

Linear MPC, as previously elaborated, capitalizes linear process models which constitute convex optimisation problems and take advantage of their deterministic nature. However, in general control engineers deal with systems with a non-linear behaviour and therefore cannot be formulated as convex optimisation problems [62, 78].
Nonlinear MPC would require a tremendous computationally effort in its application [78]. Fuzzy predictive controller don't differ essentially in their design structure from regular model-based fuzzy design approaches [55]. Takagi-Sugeno fuzzy models offer a potent solution to circumvent a non-linear MPC modeling [79, 80, 81, 78].

FMPC can be viewed as a parallel connection of a number of linear MPC, having identical settings in terms of prediction horizon, control horizon, sampling time and constraints [36, 44], along the series of operating point within a local linear model network 3.3. In order to determine the individual MPCs, the the underlying non-linear model structure has to be linearized, if mathematically formulated, or identified via black box modeling.

For the Takagi-Sugeno framework, a membership function for the fuzzification phase has to be chosen. Trapezoidal, triangular or Gaussian can be considered, to assign each MPC to its respective operating regime. Both ways of interpolating between the local MPCs are conceivable - blending outputs 3.4 and blending parameters 3.5.

Mathematically, the model predictive control scheme 3.44, 3.45 is inserted into the Takagi-Sugeno template 3.24 which yields to

$$\begin{aligned} R^i\text{: IF } & y_1 \in A_1^i \wedge ... \wedge y_m \in A_m^i \\ & \text{THEN } \boldsymbol{u}_i(k) = -\boldsymbol{K}_{mpc,i}\boldsymbol{x}(k) + \boldsymbol{K}_{y,i}\boldsymbol{y}_{ref}(k) \end{aligned} \tag{3.58}$$

where R^i denotes the i-th fuzzy rule, y_1,..., y_m are the output variables, A_i and B_i are the system matrix and the input matrix of each linear local model and A_m^i are fuzzy sets associated to a respective membership function $\mu_{A_m}^i(x_m)$ where $i = 1,..., n$ and $j = 1,..., m$.
The output of fuzzy model-based predictive controller

$$\boldsymbol{u}(k) = \sum_{i=1}^{n} \Phi \boldsymbol{u}_i(k) \tag{3.59}$$

is a linear combination of the outputs of the local MPCs which is determined with each time step depending on their individual membership in the current fuzzy regime in a receding horizon manner.
Graphically, the control configuration of a FMPC is represented in fig. 3.7. There, a three parallel model-based predictive controllers with an identical structure, being output blended by a Takagi-Sugeno fuzzy model-based arrangement, is shown (compare fig. 3.3). One of the outputs y_4 is being used to determine to which degree each MPC contributes to the superposed output of the FMPC.

3.5.1 Stability of FMPC

The stability of the FPMC is based on the Lyapunov theorem similarly to the case of an ordinary MPC [34]. Yet, unlike the Lyapunov candidate of the stability proof for a

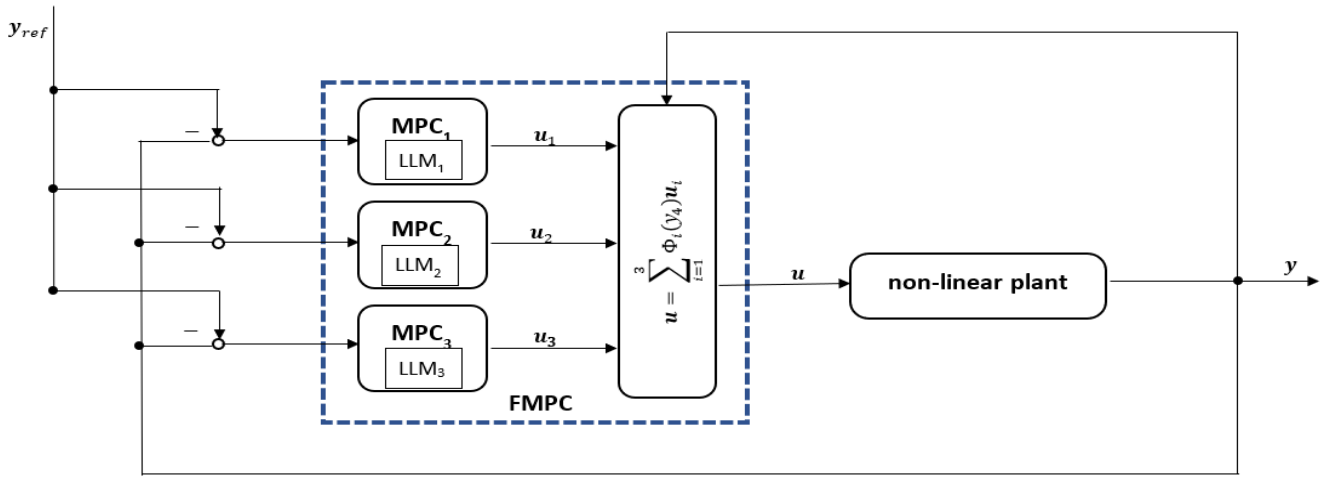

Figure 3.7: Control structure of a FMPC with three linear local models

single MPC, the closed loop system matrix $(\boldsymbol{A} - \boldsymbol{B}\boldsymbol{K}_{mpc})$ of the closed-loop state space equation of the individual MPC and their permutations is investigated. According to the stability theorem, a common P has to exist which proofs stability of the Takagi-Sugeno system for which a linear matrix inequality is to fulfill [69].

Theorem 2 *The equilibrium of the discrete fuzzy system with* $\boldsymbol{u}(t) = 0$ *is globally asymptotically stable if there exists a common positive matrix* $\boldsymbol{P}$ *such that*

$$\boldsymbol{A}_i^T \boldsymbol{P} \boldsymbol{A}_i - \boldsymbol{P} < 0, i = 1, 2, ..., n \tag{3.60}$$

that is, common $\boldsymbol{P}$ *has to exist for all subsystems [34].*

Now, the system matrix of the closed loop augmented system 3.47 is inserted into 3.60 which yields to

$$(\boldsymbol{A}_i - \boldsymbol{B}_i \boldsymbol{K}_{mpc,j})^T \boldsymbol{P} (\boldsymbol{A}_i - \boldsymbol{B}_i \boldsymbol{K}_{mpc,j}) - \boldsymbol{P} < 0, i, j = 1, 2, ..., n. \tag{3.61}$$

Finally, each consequent part of the Takagi-Sugeno fuzzy rule of the FMPC has to be permuted with each MPC. Everyone of those permutations need to satisfy the linear matrix inequality. This resembles the interconnections among the local linear models and hence proofs stability for the whole closed-loop system.
Even though, the term $\boldsymbol{B}\boldsymbol{K}_y \boldsymbol{y}_{ref}(k)$ is not $\boldsymbol{0}$, it is still bounded and therefore the stability proof remains its validity [69].

Chapter 4

Control Design

4.1 The State Space System

The mechanical behaviour of the analogous model, the Hybrid Synergy Drive, was mathematically described by the framework of Lagrange mechanics. In total, a system of four ordinary, linear, first order differential equations

$$\Delta\dot{\phi} = \omega_3 - \omega_4, \tag{4.1}$$

$$\begin{aligned}\dot{\omega}_1 = &-\frac{M_2}{M_5 M_1} k_s(\phi_3 - \phi_4) - \frac{M_2}{M_5 M_1} d_s(\omega_3 - \omega_4) + \\ &+ \frac{1 + \frac{M_2 M_3}{M_1 M_5}}{M_1} T_{Eng} + \frac{(\frac{2r_1}{r_2} + \frac{M_2}{M_5}(\frac{2r_1 M_3}{r_2 M_1} - \frac{r_3}{r_2}))}{M_1} T_{MG1} + \frac{M_2}{M_5 M_1} T_{MG2},\end{aligned} \tag{4.2}$$

$$\begin{aligned}\dot{\omega}_3 = &-\frac{M_2}{M_5 M_1} k_s(\phi_3 - \phi_4) - \frac{M_2}{M_5 M_1} d_s(\omega_3 - \omega_4) + \\ &+ \frac{M_3}{M_1 M_5} T_{Eng} + \frac{(\frac{2r_1 M_3}{r_2 M_1} - \frac{r_3}{r_2})}{M_5} T_{MG1} + \frac{1}{M_5} T_{MG2},\end{aligned} \tag{4.3}$$

$$\dot{\omega}_4 = \frac{1}{J_4} k_s(\phi_3 - \phi_4) + \frac{1}{J_4} d_s(\omega_3 - \omega_4) - \frac{1}{J_4} T_{Load} \tag{4.4}$$

make up the linear system. In order to meet the requirements of the similarity approach, a non-linear spring parameter

$$k_s(\omega_4) = c_2 \omega_4^2 + c_1, \tag{4.5}$$

is introduced, to transform the original system to a non-linear system. The state space formulation is constituted by the state vector

$$\boldsymbol{x} = \begin{bmatrix} \Delta\phi_{34} & \omega_1 & \omega_3 & \omega_3 \end{bmatrix}^T,$$

consisting of the difference of the rotation angles around the spring-damper element in [rad], the rotational speed of the combustion engine in $[s^{-1}]$, the rotational speed of the first motor generator and the rotational speed of the second motor generator in $[s^{-1}]$, by the input vector

$$\boldsymbol{u} = \begin{bmatrix} T_{eng} & T_{MG1} & T_{MG2} \end{bmatrix}^T,$$

which contains the torque of the combustion engine in [Nm], the torque of the first and the second motor generator in [Nm], by the disturbance vector

$$z = T_{Load},$$

which is equal to load torque in [Nm], and by the output vector

$$\boldsymbol{y} = \begin{bmatrix} \omega_1 & \omega_4 \end{bmatrix}^T$$

being elected to be the rotational speed of the combustion engine in $[s^{-1}]$ and of the load mass in $[s^{-1}]$. By setting everything in and gathering the parameters, the non-linear LTI system

$$\dot{x}_1 = x_3 - x_4, \tag{4.6}$$
$$\dot{x}_2 = -K_1 x_1 x_4^2 - K_2 x_1 - K_3(x_3 - x_4) + K_4 u_1 + K_5 u_2 + K_6 u_3, \tag{4.7}$$
$$\dot{x}_3 = -K_7 x_1 x_4^2 - K_8 x_1 - K_9(x_3 - x_4) + K_{10} u_1 + K_{11} u_2 + K_{12} u_3, \tag{4.8}$$
$$\dot{x}_4 = K_{13} x_1 x_4^2 + K_{14} x_1 + K_{15}(x_3 - x_4) - K_{16} z \tag{4.9}$$

is obtained with K_1, K_7, K_{13} in $[s^{-4}]$, K_2, K_8, K_{14} in $[s^{-2}]$, K_3, K_9, K_{15} in $[s^{-1}]$ and K_4, K_5, K_6, K_{10}, K_{11}, K_{12}, K_{16} in $[kg^{-1}m^{-2}]$. The resulting non-linear MIMO system has three inputs, four states, one disturbance and two outputs.

4.2 Analysis of System Dynamics

For design of the control algorithm, an analysis of the system dynamics has be carried out which is inspired by the studies of Wang [82, 83, 84, 85, 86] who dedicated his research activities on the topic of control engineering on helicopters with variable rotor speed. His contributions on non-linear model predictive control offer a solid foundation for the undertaking of the control design.
A promising finding to approach his work was that due to different parameter settings of the model, the dynamic behaviour shows a differs significantly. Along the three system parameters rotational speed, altitude and forward speed, a monotonic shift in the

natural frequency was observable, in case of an isolated contemplation of this parameter.
Now, a similar system behaviour was simulated for the analogous model. The angular rotational speed of the load mass which has a non-linear influence on the system behaviour was varied in such a way that a required frequency range was covered.
In comparison to Wang, instead of a three-dimensional parameter space only a single parameter exerts influence on the dynamical behaviour of the plant which significantly simplifies the control design.
In terms of partitioning, a more superior approach was at least intended to be adopted by applying the ν gap metric to evaluate the distance between the individual models by the partition variable ω_4 within the operation space of instead of using equidistant points. Similarly, a model-based predictive controller was applied. In our case a fuzzy MPC was used which circumvents a non-linear processing of the system but rather chooses a set of operating points and interpolates between them, under the assumption that a particular point between two operation points can be determined by interpolation.
An operation regime of the analogous model was decided to be taken such that the natural frequencies of would appear within the regime of $2-5$ Hz in accordance to the original rotor-craft model of the UH-60.
The partition of the prior operation space was carried out by backward regression. Initially, the ν gap metric was applied and implemented by the Algorithm 1 which was suggested by [48]. With an $\epsilon = 0.4$ a number of 32 models in the partitioning space were obtained. The results can be found in tab. 4.1. This outcome was unexpected and unsatisfactory due to the high amount of models and therefore higher complexity in the latter design of the FMPC.

Algorithm 1 ν gap partitioning algorithm

1: Equidistant partition of the operation space in n models (where n is "not too big")
2: Linearization of the non-linear system at those operation points according to the scheme $Op_i = (x^i, f(x^i))$ with $i = 1, ..., n$
3: Determine the distance according to the ν gap metric
4: **while** $\delta_k = \delta(G_k, G_{k+1}) = max_{i=1}^{n-1}\delta_i > \epsilon$ **do**
5: Create a new operation point $Op_{new} = G_k + \frac{G_{k+1}-G_k}{2}$
6: Determine the new ν gap value between $G_{k,new}$ and G_k, and $G_{k,new}$ and G_{k+1}
7: **end while**

OP_i	OP_{i+1}	ν gap	k($\omega_{4,i}$)	k($\omega_{4,i+1}$)	$\omega_{4,i}$	$\omega_{4,i+1}$
1	2	0,18	50,00	51,70	0,00	2,92
2	3	0,49	51,70	56,80	2,92	5,83
3	4	0,36	56,80	60,63	5,83	7,29
4	5	0,42	60,63	65,30	7,29	8,75
5	6	0,47	65,30	70,83	8,75	10,20
6	7	0,27	70,83	73,91	10,20	10,93
7	8	0,28	73,91	77,20	10,93	11,66
8	9	0,29	77,20	80,71	11,66	12,39
9	10	0,30	80,71	84,43	12,39	13,12
10	11	0,31	84,43	88,36	13,12	13,85
11	12	0,32	88,36	92,50	13,85	14,58
12	13	0,32	92,50	96,86	14,58	15,31
13	14	0,33	96,86	101,43	15,31	16,04
14	15	0,34	101,43	106,21	16,04	16,76
15	16	0,34	106,21	111,20	16,76	17,49
16	17	0,35	111,20	116,41	17,49	18,22
17	18	0,36	116,41	121,83	18,22	18,95
18	19	0,36	121,83	127,46	18,95	19,68
19	20	0,36	127,46	133,30	19,68	20,41
20	21	0,37	133,30	139,36	20,41	21,14
21	22	0,37	139,36	145,63	21,14	21,87
22	23	0,38	145,63	152,11	21,87	22,59
23	24	0,38	152,11	158,80	22,59	23,32
24	25	0,38	158,80	165,71	23,32	24,05
25	26	0,39	165,71	172,83	24,05	24,78
26	27	0,39	172,83	180,16	24,78	25,51
27	28	0,39	180,16	187,70	25,51	26,24
28	29	0,39	187,70	195,46	26,24	26,97
29	30	0,40	195,46	203,43	26,97	27,70
30	31	0,40	203,43	211,61	27,70	28,43
31	32	0,40	211,61	220,00	28,43	29,15

Table 4.1: Partition of the operation space by the ν gap metric

A new and simpler approach was applied. Now for simplification purposes, for the partition of the operation space an euclidean metric e.g. equally distant points was chosen with a desired number of models of 4. Finally, the first model close to the lower end

of the operation regime was discarded due to its redundant nature in the participation of the overall performance of the FMPC which serves the dogma of minimal required complexity.

In fig. 4.1 a bode plot of the three models in the individual operation points is depicted. The red lines mark the required natural frequencies. The black dashed lines characterize the possible natural frequencies within the required regime. The finally chosen operation points are again subset of the previous constraints in the frequency domain.

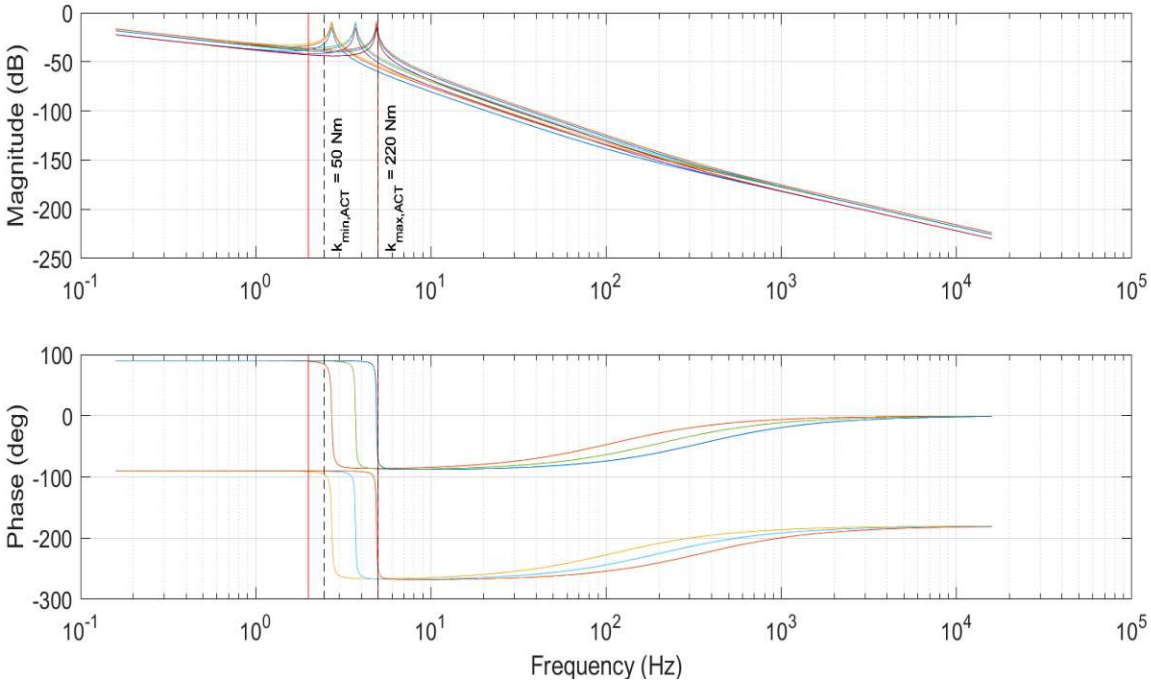

Figure 4.1: Bodeplot of linearized model along the desired frequency range

Finally, the assignment of the models along the operation regime is depicted in fig. 4.2 along the non-linear spring parameter, monotonically increasing along the rotational speed ω_4 of the reduced mass at the end of the analogous model.

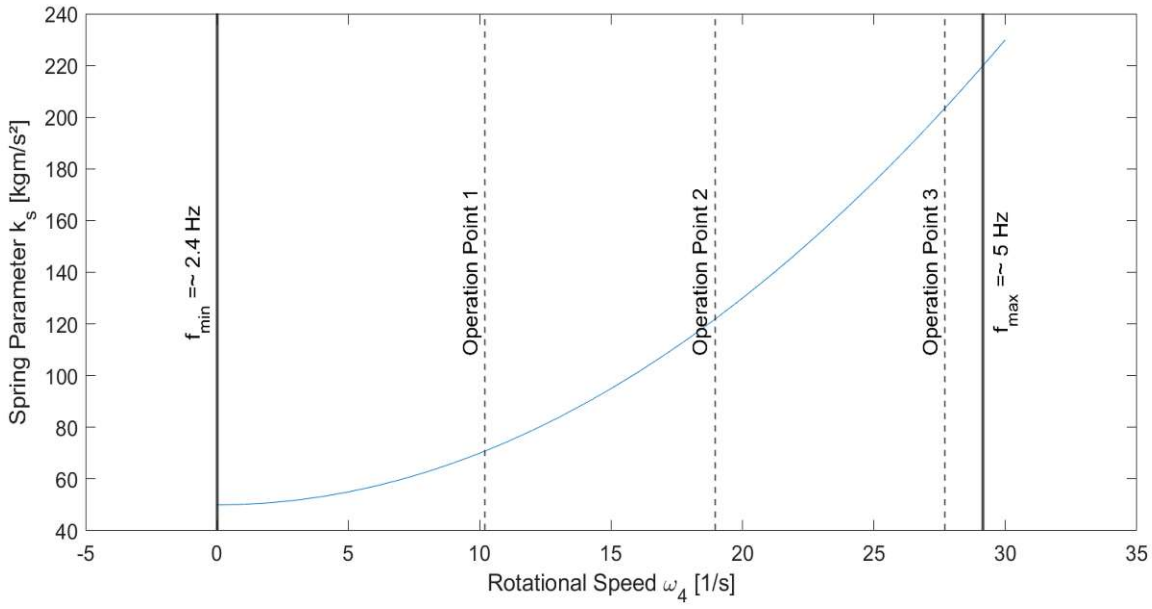

Figure 4.2: Characteristic curve of the spring parameter and the three operation points

4.3 The Design of the FMPC

The FMPC was obtained by output blending which allows a simpler implementation than parameter blending. For the fuzzification phase, trapezoidal membership functions and for the defuzzfication weighted average method were chosen. The close vicinity of the operation points constitutes the fuzzy sets which make up the fuzzy interference system.

For the design of the FMPC and the individual MPCs, a sampling time of $t_s = 0.002$ s was chosen. The prediction horizon and the control horizon were set to be $Np = 50$ and $Nc = 15$, respectively. Finally, the weighting matrices of the FMPC and the individual MPCs was chosen to be

$$Q = \begin{bmatrix} 82500 & 0 \\ 0 & 825000 \end{bmatrix}, \; R = \begin{bmatrix} 1 & 0 & 0 \\ 0 & 1 & 0 \\ 0 & 0 & 1 \end{bmatrix}.$$

The following hard constraints

- 1000 rpm $-$ 4500 rpm on the first state ω_1 to ensure a high efficiency factor and

- -800 Nm $-$ 800 Nm on the three inputs T_{Eng}, T_{MG1} and T_{MG2} to mimic the behaviour of an ordinary motor vehicle

were imposed. The further constraints was applied to all the simulations, whereas the latter one was used for one specific simulation experiment.

The membership functions of the Takagi-Sugeno fuzzy template are shown in in fig. 4.3. The trapezoidal membership function have the advantage of assigning sole validity of an individual model in the close vicinity of its operation point.

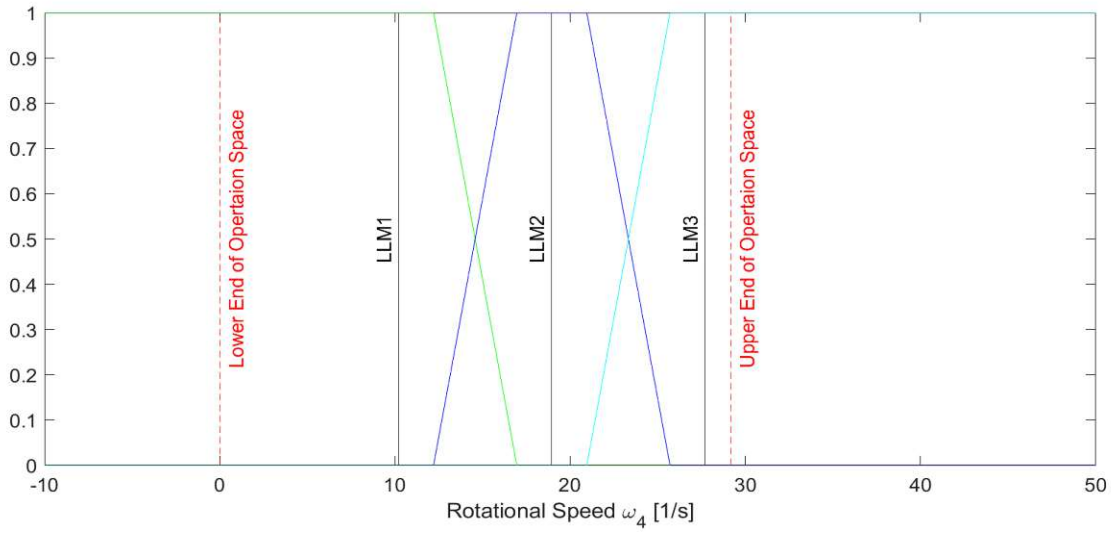

Figure 4.3: Trapezoidal membership functions of the FMPC

Chapter 5

Results

Finally, the simulation results are going to be presented here for the FMPC of the analogous model for UH-60 helicopter. Therefore, a series of simulation experiments were conducted to validate and verify the closed-loop behaviour of the FMPC in terms of the rotational speed of the load mass ω_4. Meanwhile ω_1, the rotational speed of the combustion engine, was not excited. Yet, its variation range was constraint to ensure a high efficiency factor in case of coupling effects among the state variables.
Initially, the closed-loop behaviour along the set of operation points were validated to be stable. Therefore, the performance of the MPC operating on the linearized plant in the individual operating point, the MPC operation on the non-linear plant and the FMPC were compared. Secondly, the stable behaviour of the FMPC on the region between two individual operation point was verified. Thirdly, the design of the local linear model network was validated by exploring the system behaviour on the operation space of and around the discarded local linear model.
Fourthly, the validation of the transient behaviour between the operation points of the FMPC was investigated. Additionally, the setting of hard constraints on the amplitude on all system inputs were tested. Sixthly, a predictive disturbance suppression of the FMPC was tested against an FMPC without that additional implementation. Thereafter, the stability of the FMPC was investigated by Lyapunov.

5.1 Validation of the individual Operating Points

The first simulation experiment was conducted to validate the individual operation points. Therefore, the behaviour of the MPC on the linearized plant, the MPC on the non-linear plant and the FMPC were validated in the close vicinity around the operation points.
So, a positive step of a small size in comparison to the set point signal was applied in a steady state. After $1s$, another small but negative step of double size was performed

and finally a positive step back to the original value of the set point was carried out. The results are as expected. For every operation point, the control performances of the individual controllers are congruent with each other which verifies the correct implementation of the procedure. All of the controllers are stable and perform naturally without a steady state error. The damping is congruent with requirement. the controller acts sufficiently fast.
The hard constraints on the first system output y_1 was not activated. So, the restrictions on it did not affect the global solution and are therefore considered to be loosely. Yet, in case two an interesting observation was done. Even though the FMPC and the MPC on the linear plant were stable for the given configuration, the MPC for the non-linear plant was not. In order to compare the result locally, the weighting matrix $\boldsymbol{Q}$ was decreased. This perfectly illustrates the non-linear effects among the MPC within the configuration of the FMPC. So to speak, the FMPC is more than the sum of its parts. The results are found in fig. 5.1, fig. 5.2 and fig. 5.3.

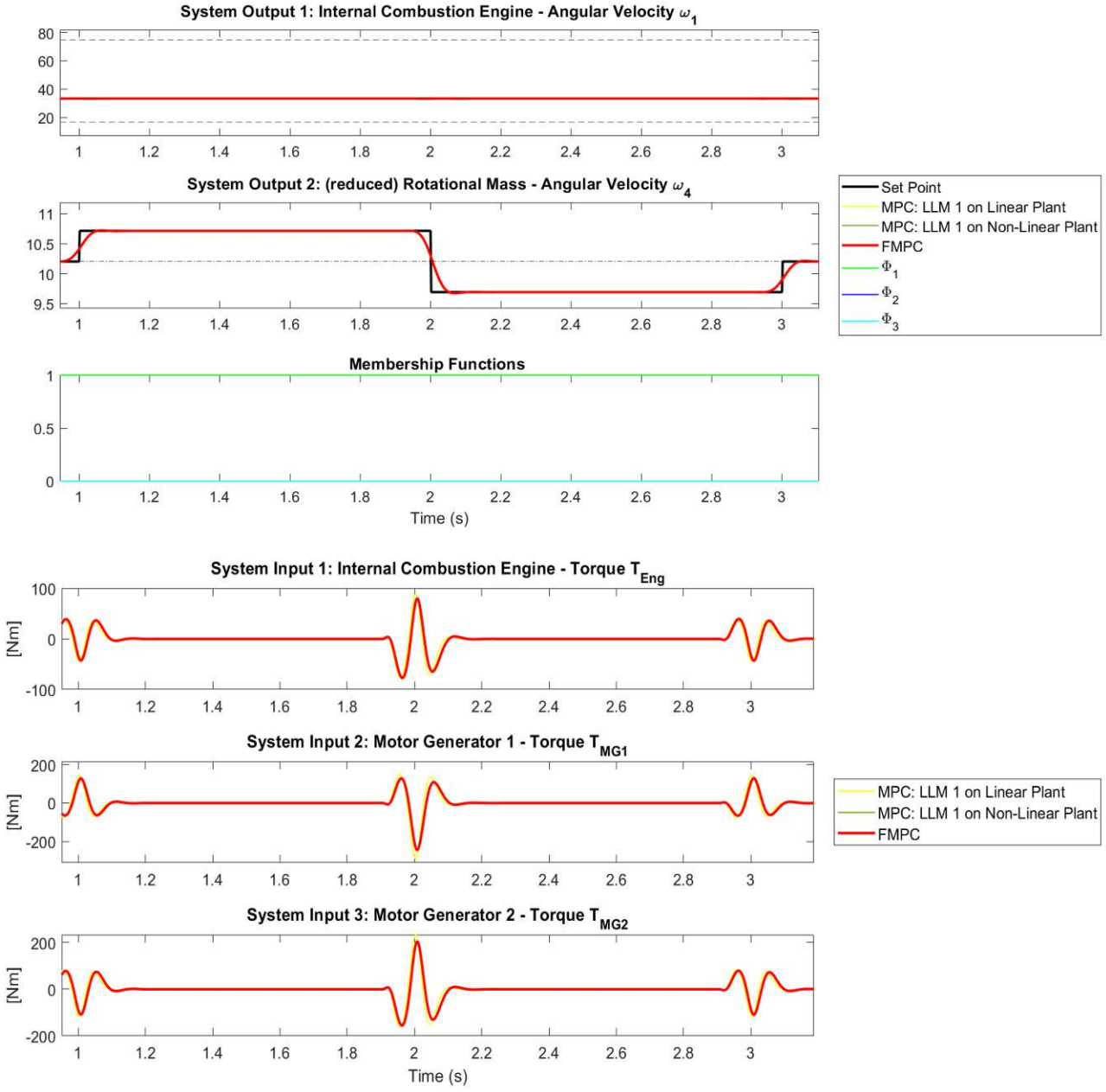

Figure 5.1: Validation the of operation point 1 by the MPC on the linear plant, the MPC on the non-linear plant and the FMPC. The dashed line marks the constraints on ω_1 and the dash-dotted line the OP 1. All three input and output of all three controllers a overlapping. It can be seen that only the first membership function is activated while the others a set to zero.

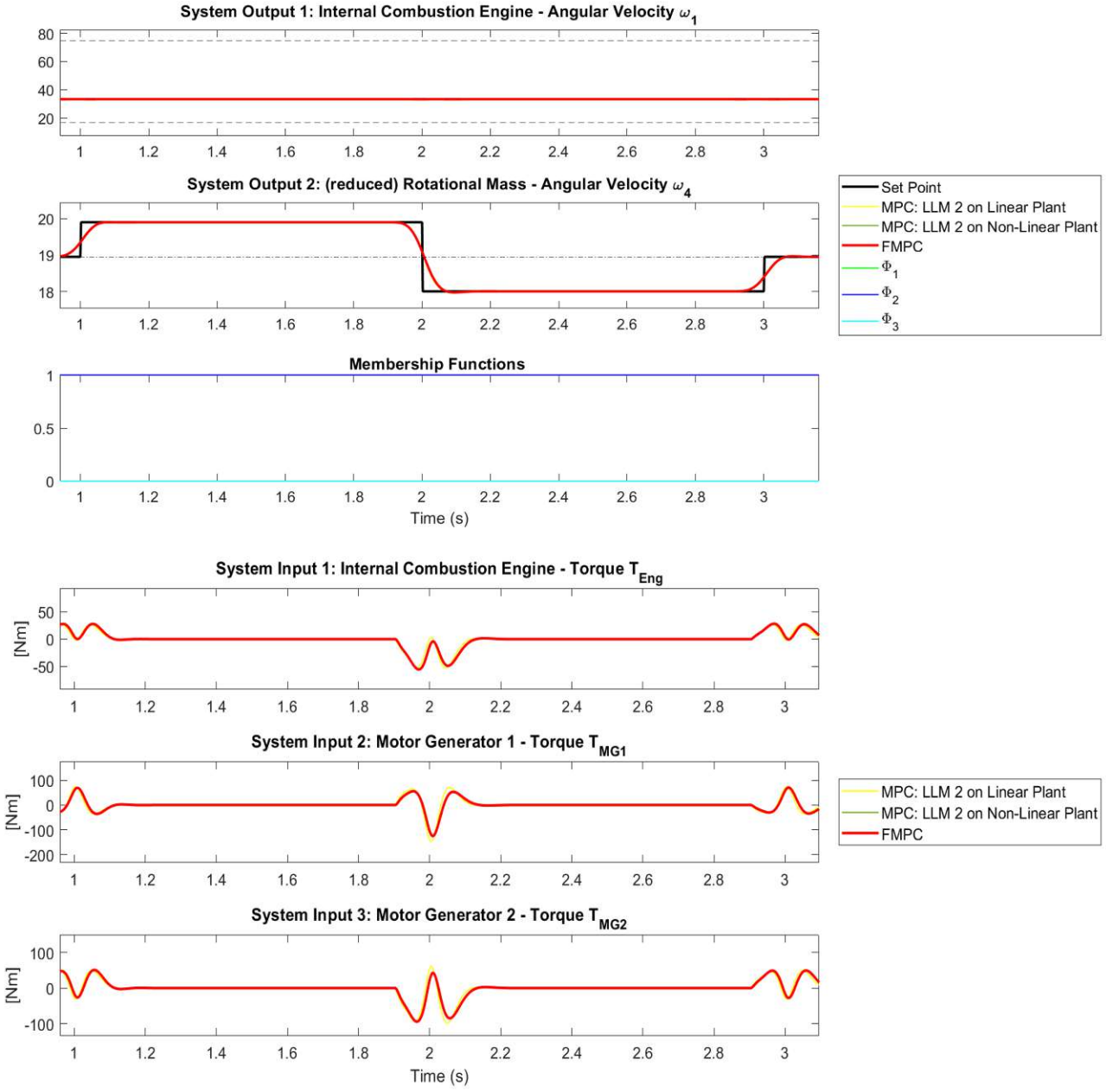

Figure 5.2: Validation of operation point 2 by the MPC on the linear plant, the MPC on the non-linear plant and the FMPC. The dashed line marks the constraints on ω_1 and the dash-dotted line the OP 2. All three input and output of all three controllers a overlapping. It can be seen that only the second membership function is activated while the others a set to zero.

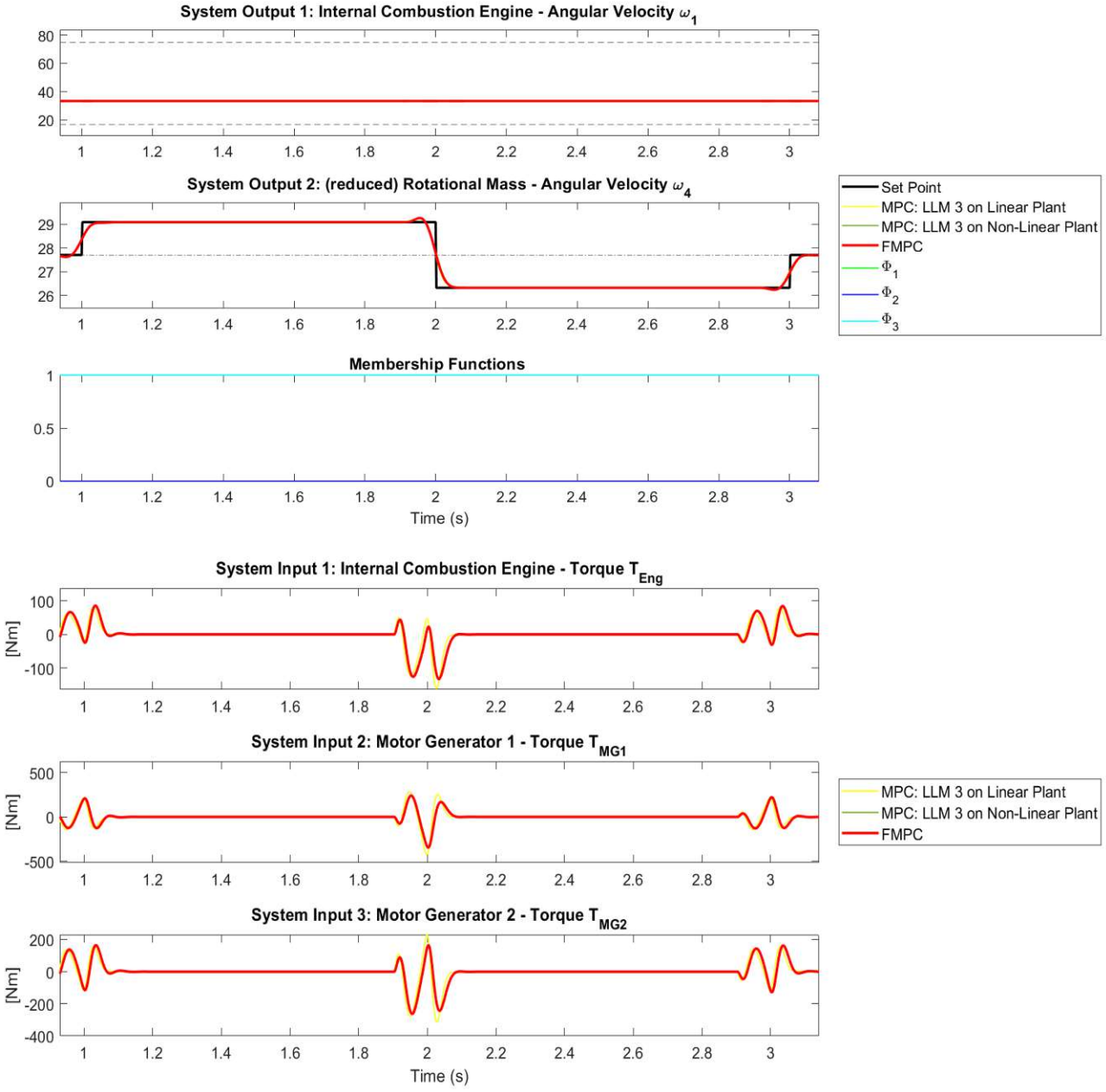

Figure 5.3: Validation of operation point 3 by the MPC on the linear plant, the MPC on the non-linear plant and the FMPC. The dashed line marks the constraints on ω_1 and the dash-dotted line the OP 3. All three input and output of all three controllers a overlapping. It can be seen that only the third membership function is activated while the others a set to zero.

5.2 Validation of the Area between the Operation Points

For the second series of experiments, the control performance and stability was validated in the more wider region around the operation points. It was intended to activate to the MPCs on two adjacent operation points.
Again, the FMPC is stable and performs without a steady state error. The damping is satisfyingly and its predictive nature is perfectly visible. The FMPC is sufficiently fast. Similarly, the hard constraints on the system output y_1 were not touched and therefore did not play a role in the final solution.
As expected the control behaviour of the FMPC is a superposition of the individual ones which is indicated by the activated membership functions. It is worth noticing that u_1 and u_2, the torque for the first and second motor generator, adopt values close to 1000 Nm, in sense of a real value, which is slightly exceeding the operation range of an ordinary motor vehicle. In the following simulation experiment, this will be investigated more deeply. The results can be found in fig. 5.4 and fig. 5.5.

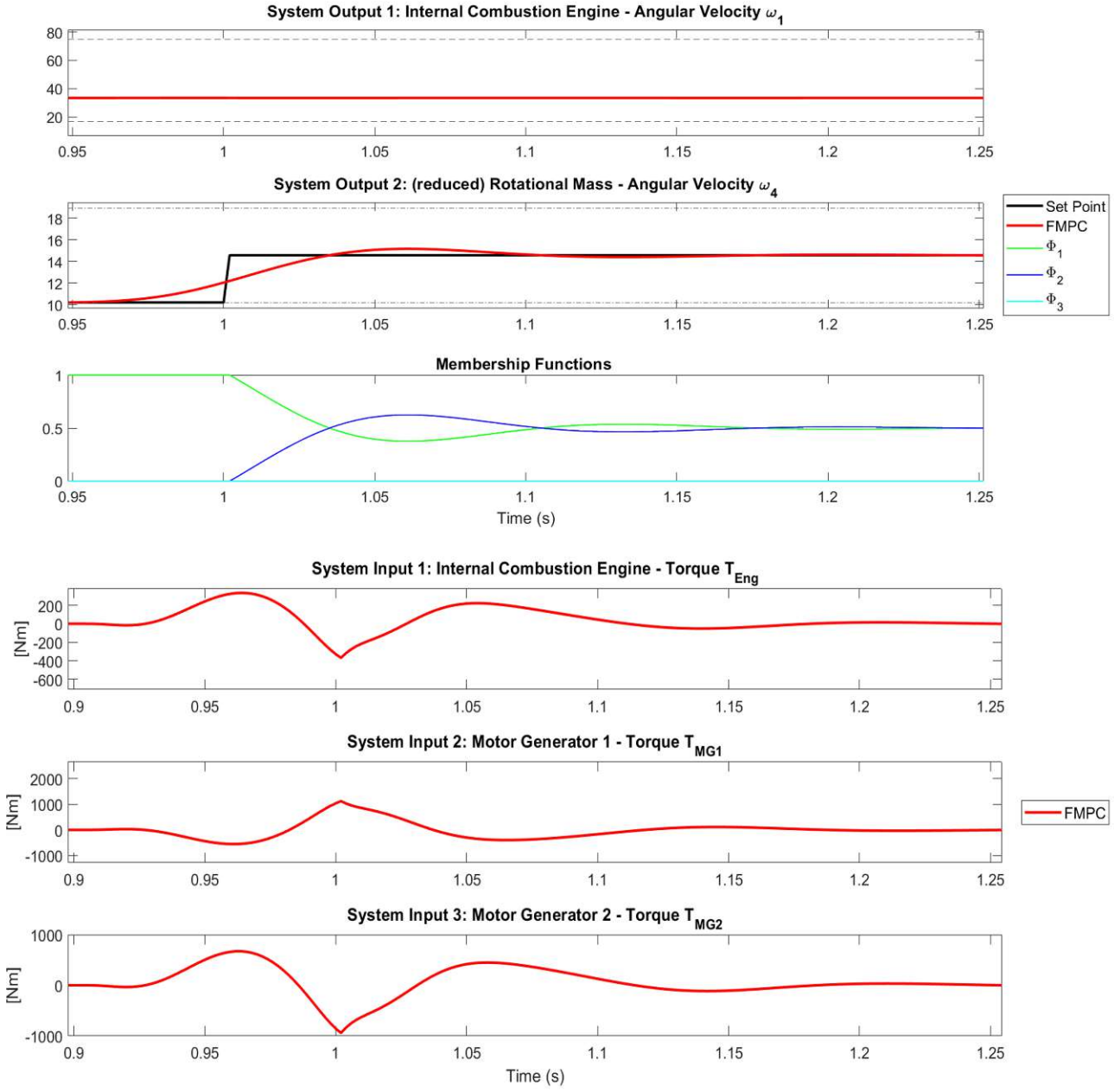

Figure 5.4: Validation of the region between the operation points 1 and 2. The dashed line marks the constraints on ω_1 and the dash-dotted line the adjacent OP 1 and OP 2. As expected, the two adjacent MPCs are activated while the third one is inactive.

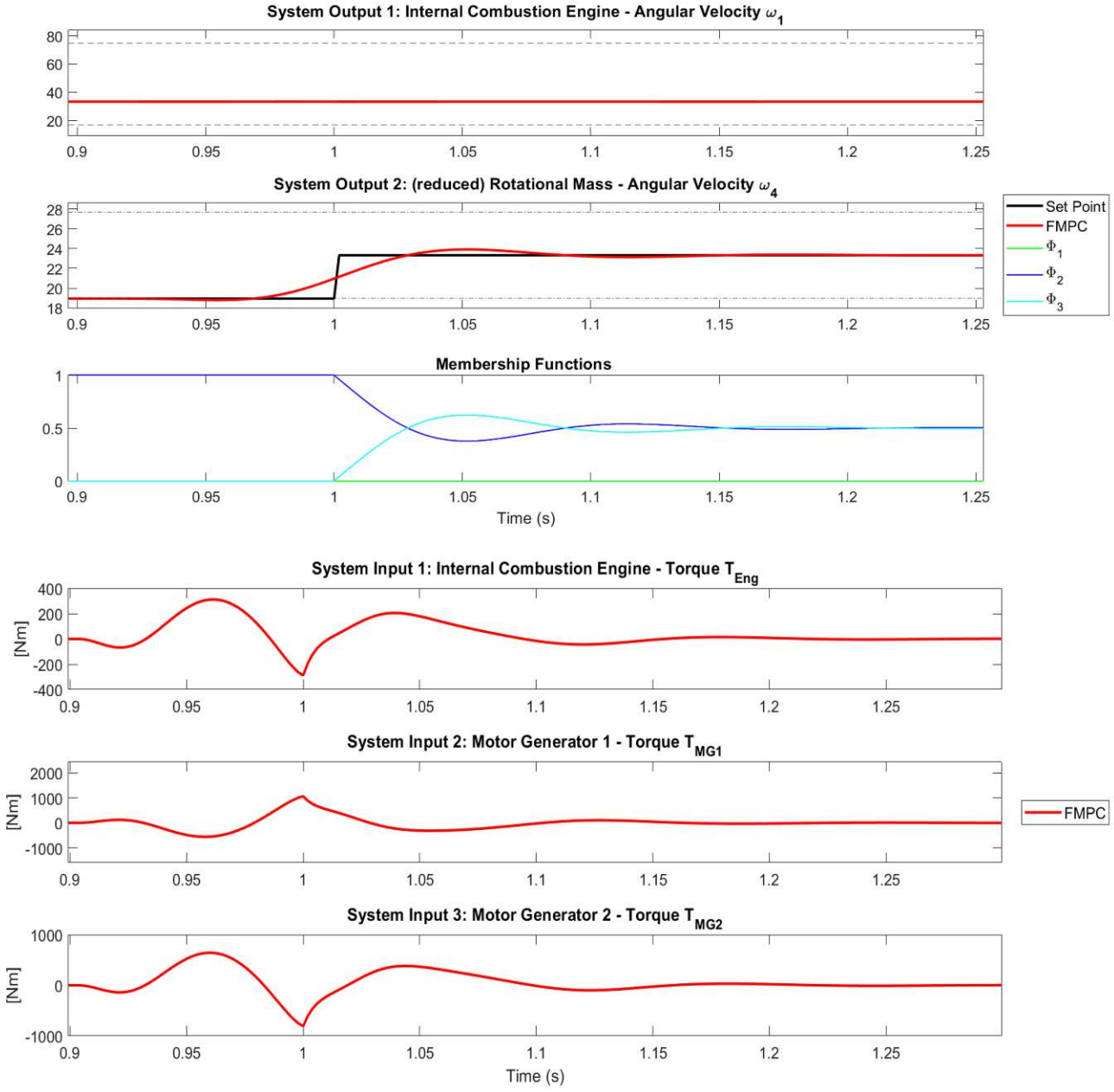

Figure 5.5: Validation of the region between the operation points 2 and 3. The dashed line marks the constraints on ω_1 and the dash-dotted line the adjacent OP 2 and OP 3. As in the prior experiment, the two adjacent MPCs are activated while the first one is inactive.

5.3 Validation of the Design Procedure

Additionally, the region below the first operation point was investigated to verify the design decision of only three operation points and discarding the one in the lower operation space. In order to do that a simulation experiment was conducted in that region to figure out whether the FMPC stays stable and performs satisfyingly. As in the previous examples were the hard constraint on y_1 not touched.
Again, the predictive nature of the FMPC was shown. The controller performs without a steady state error and is well damped. The results demonstrate that another model is not essentially required and that the model in the currently first operation point covers the region below its validity space. The results can be found in fig. 5.6.

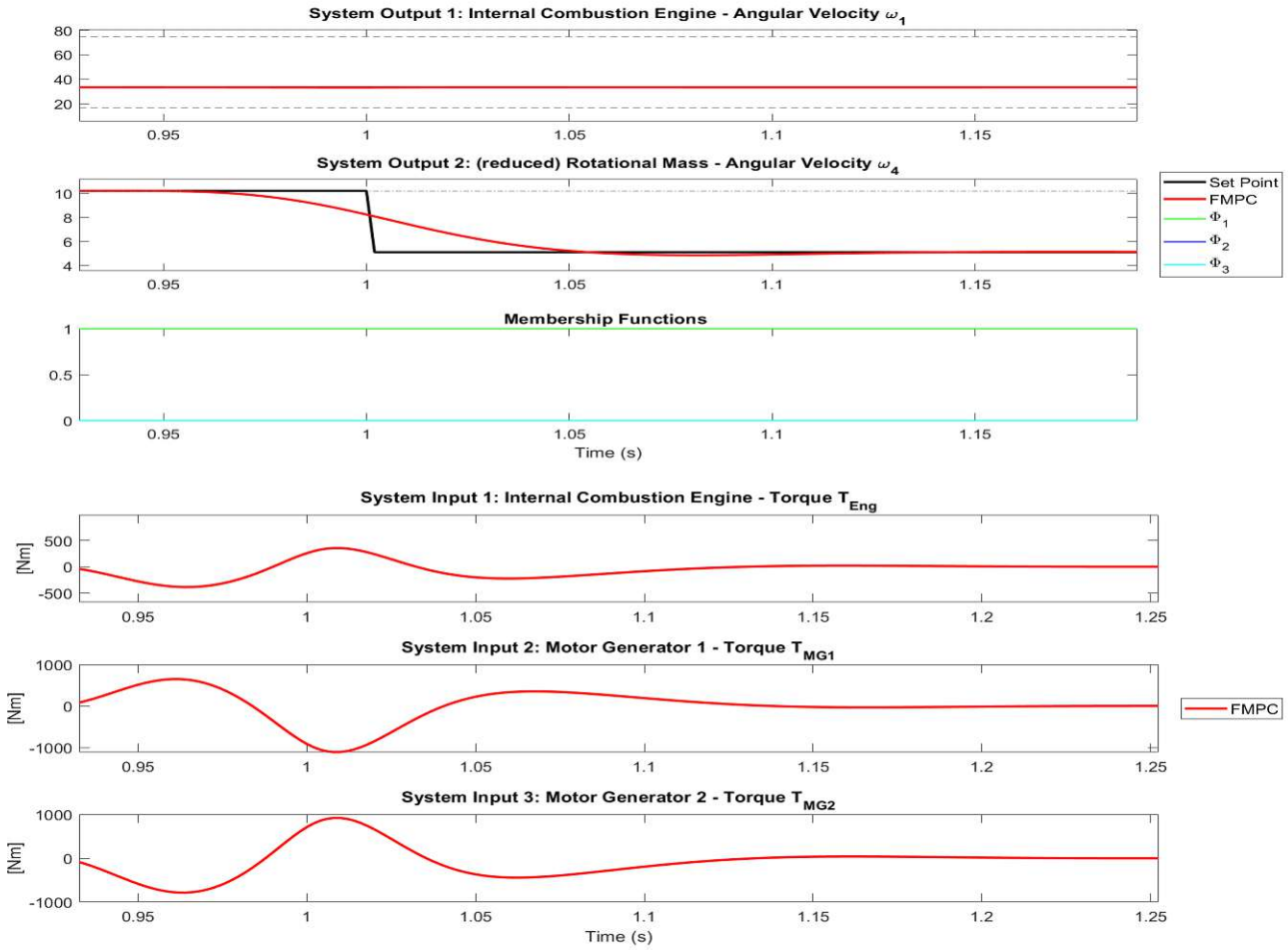

Figure 5.6: Validation of the FMPC performance region below operation point 1. The dashed line marks the constraints on ω_1 and the dash-dotted line the OP 1. The pathway of the membership functions show that only the first model is activated.

5.4 Validation of the transient Behaviour

Finally, the transient behaviour of the FMPC on the plant of the non-linear analogous model was investigated. Therefore, step changes along the operation points were conducted to trigger the changes in the active models of the FMPC.
This simulation experiment is considered as potentially problematic since off-equilibrium problems dynamics might lead to unwanted effects. Anyways, the transient behaviour can be seen perfectly among the membership functions. The FMPC performs again as desired. Again, the hard constraints on y_1 were not used.

This result shows that the operation points are not located to distinct apart. It is noticeable that the control action, especially, for the torque of the first motor generator is extremely high and are not performed by conventional vehicles. Hence, hard constraints on the amplitude of the system inputs are goint to be imposed. The results can be found in fig. 5.7.

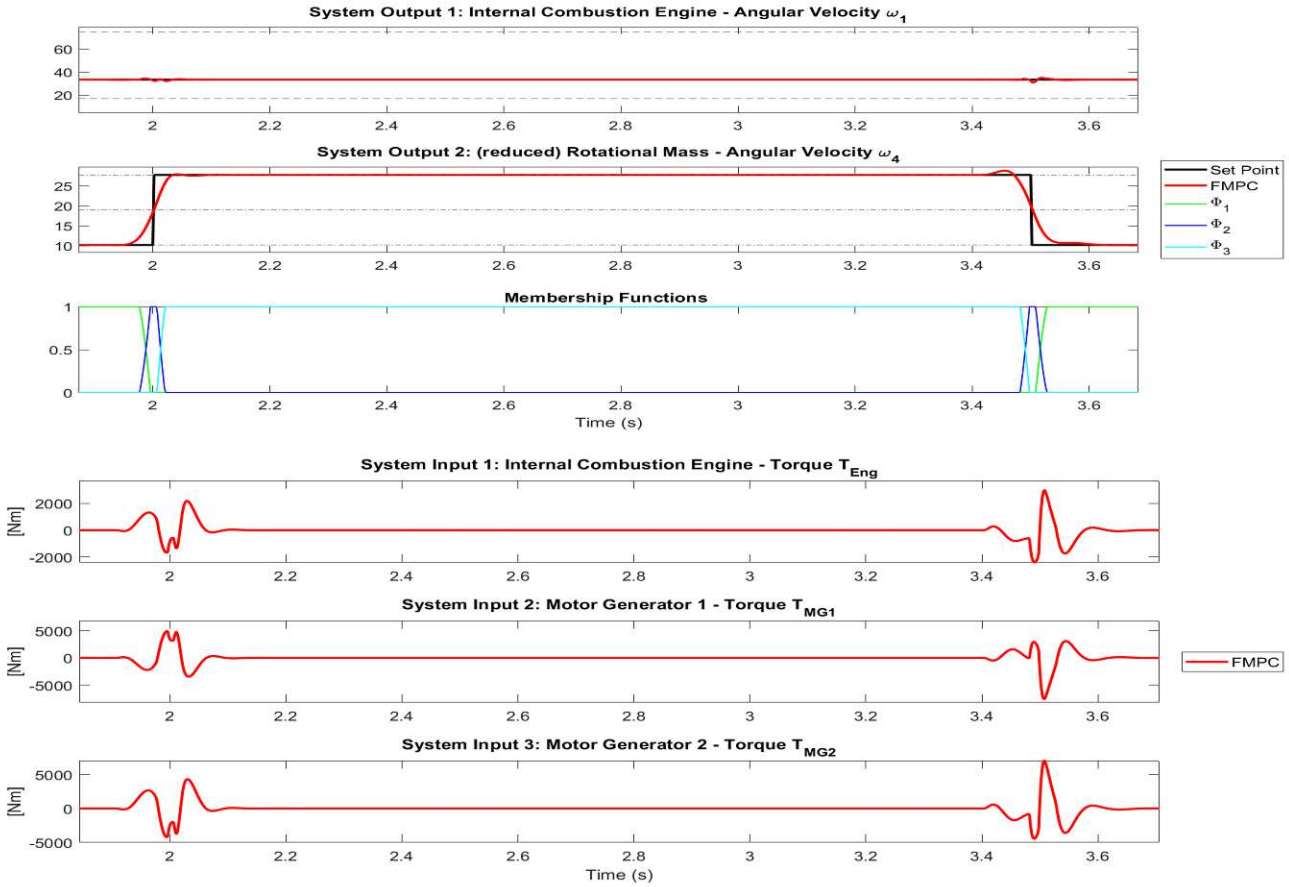

Figure 5.7: Validation of the transient behaviour of the FMPC. The dashed line marks the constraints on ω_1 and the dash-dotted line the three OP. Activation of all three membership functions perfectly show the transient behaviour along the three operation points (highlighted by the dashed line)

5.5 Constraint on the amplitude of the Input Variable

In order to prevent too high amplitudes in the system input, constraints were imposed. This was done for every MPC individually. This leads to the weak point of this method. By superimposing the optimally generated and constraint output (input for the non-linear system), global constraints may not be adhered to.
In fig. 5.8 it can be observed that the imposed constraints on the input (of the individual MPC) opposing to those of the system output have an impact in the stationary phases. Yet, the transient behaviour can not be constraint. This is tightly associated to the phenomenon of off-equilibrium dynamics. Too aggressive changes in the set-point signal within a transient phase may lead to dynamics which can not be seen in a stationary operation regime. Additionally, it is assumed that the region between two local linear models can be interpolated by the adjacent models.
This problem could be avoided by implementing a FMPC with parameter blending. Hence, the optimization problem of the total number of the MPC could be constraint which could therefore lead to a more satisfying result. Anyways, for a non-linear plant this can still be a challenging task.
However, the behaviour of a motor vehicle in terms of the system input could be approximately simulated. The torque of the combustion engine and of the motor generators remains below 800 Nm and would only for a short time frame violate those constraints. The price to pay for a compliant behaviour of the system input is the loss of a sufficient damping. A significant overshoot is visible on the first change of the set-point variable. For the second change (back to the value of the first OP) an even worse damping behaviour can be seen. Also, an insignificant oscillation of the first system output can be observed.
Nevertheless, the system remains stable and operates sufficiently fast. Naturally, the FMPC performs without a steady state error. Yet, it has to be added that with the original configuration of the FMPC, in particular of the weighting matrices, a feasible solution was not possible. Hence, the $\boldsymbol{R}$ matrix had to be adjusted in that manner, that the system inputs were higher weighted than in the original setting.

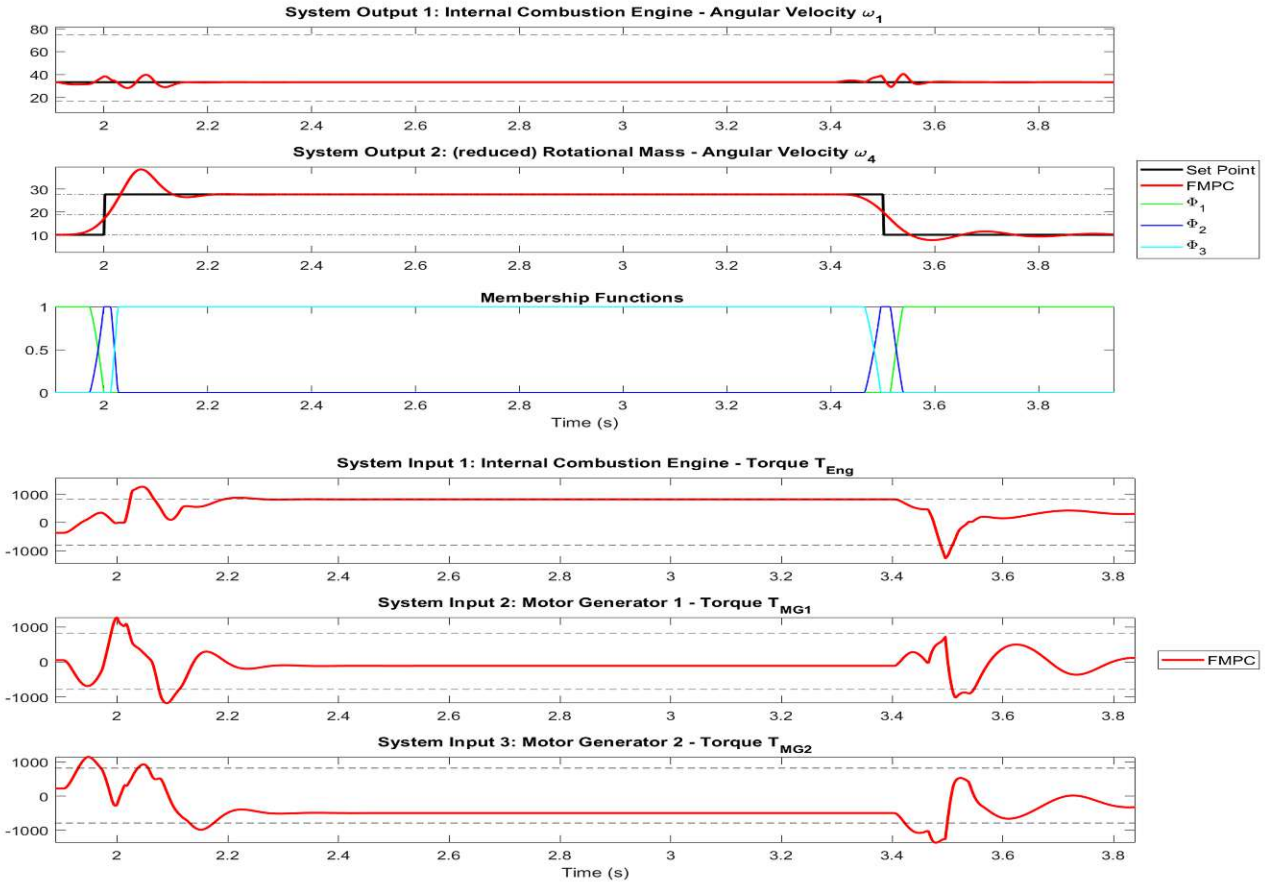

Figure 5.8: Validation of the constraint of the amplitude of the input variable. The dashed line marks the constraints on ω_1 and on T_{Eng}, on T_{MG1} and on T_{MG2}, and the dash-dotted line the three OP. Again, the transient behaviour is visible in the membership functions. The constraints of the input variable only work in the stationary operation mode.

5.6 Validation of the Predictive Disturbance Suppression

Additionally, a predictive disturbance suppression was added and opposed to a FMPC without this feature. An aggressive disturbance at $t = 2.5$ s of 333.33 Nm was applied to testify the predictive disturbance suppression of the controller. It can be perfectly seen how the one FMPC (marked by the red line) predicatively reacts as a compound of the individual MPCs (which can be seen in the behaviour of the membership functions)

to the upcoming step-wise disturbance while the other FMPC (marked by the dashed green line) is not able to act compensatory. Due to the fact that the area between operation point 1 and 2 was used for this experiment, the third membership function is inactive. The result can be found in fig. 5.9.

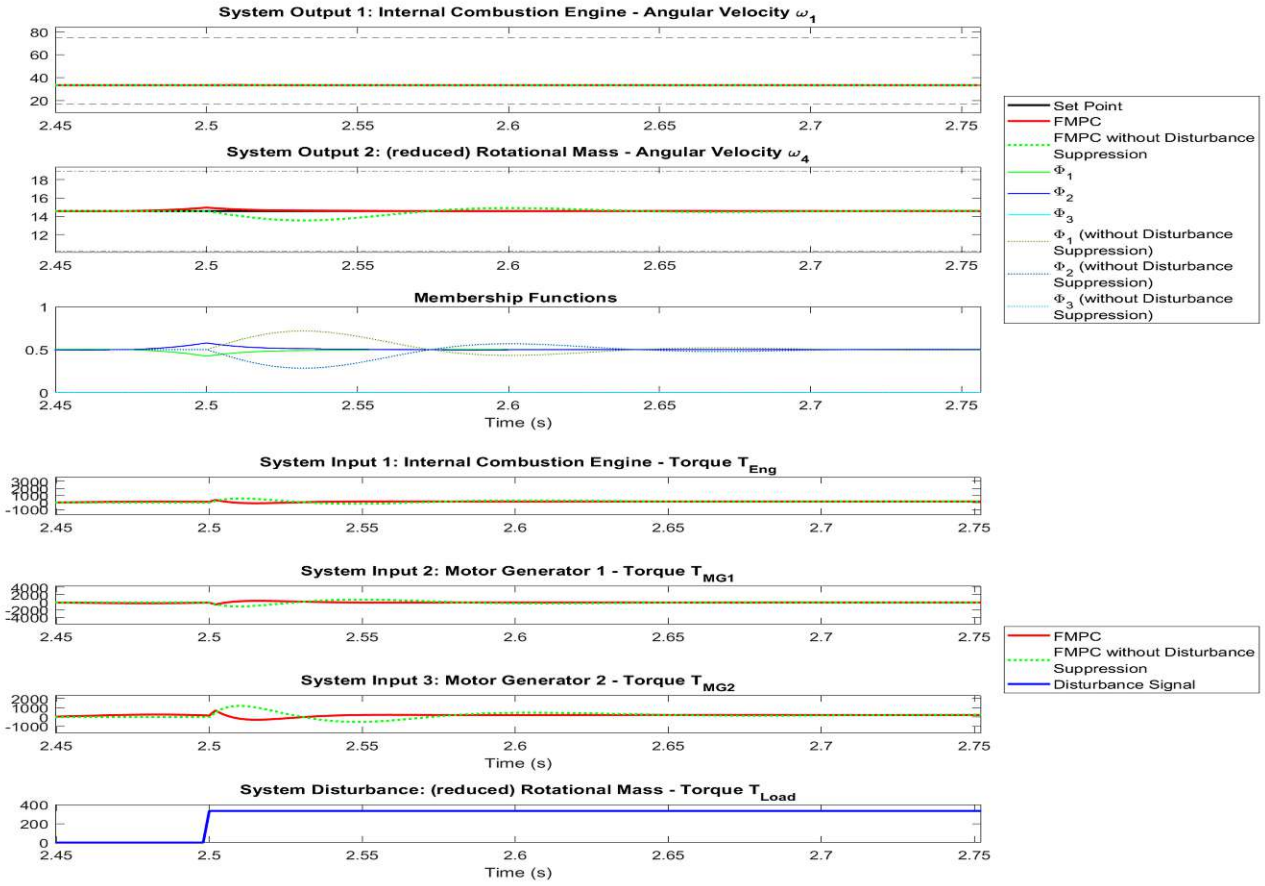

Figure 5.9: Validation of the predictive disturbance suppression the FMPC of a big stepwise disturbance. The dashed line marks the constraints on ω_1, the dash-dotted line the adjacent OP 1 and OP 2 and the dotted line the FMPC and its membership functions without disturbance suppression. The FMPC with and without disturbance suppression are depicted in comparison in the region between OP 1 and OP 2.

5.7 Evaluation of the Stability of the FMPC by Lyapunov

The stability of the FMPC is shown by Lyapunov 3.61. Therefore, the closed loop **A** matrix was selected to be a Lyapunov candidate. Even though there is an additional term including the set-point signal, this approach was still admissible due to the fact that its bounded.
All the possible open loop **A** matrices and MPC gains was permuted, which represents the interconnection of MPCs among each other. This leads to a total number of 9 LMI. MATLAB provides a set of LMI solvers. Among them the *feasp* solver was elected. Initially, for each of the linear matrix inequalities a positive definite $\boldsymbol{P}$ matrix was found but non of those $\boldsymbol{P}$ matrices could satisfy the system of LMI.
Hence, another approach was carried out. Again, the closed loop **A** matrix was chosen as a Lyapunov candidate which led to a successful result.
So, instead of searching locally for $\boldsymbol{P}$ matrix and checking each LMI individually whether they fit, a global solution was initiated. By constraining the solution space in that manner, a globally feasible solution was found.
One has to add that the original configuration was deemed by the solver to be slightly infeasible. This led to a reevaluation of possible settings of the FMPC. Finally by decreasing the predicton horizon to $N_p = 10$ and leaving the other parameters the way they were, a feasible solution was found.
However, the following Lyapunov candidate

$$P = \begin{bmatrix} \text{-84377476.48} & 1286824.87 & -387750.07 & -505672487.40 & -5443031.85 & -5178963.69 \\ 1286824.87 & 7186544.22 & -9954.94 & 1095052.64 & -3360563.53 & -976204.25 \\ -387750.07 & -9954.94 & -4237.23 & 1287028.15 & 17646.90 & 745716.11 \\ -505672487.40 & 1095052.64 & 1287028.15 & -600054355.00 & -2595023.94 & -2291577.37 \\ -5443031.85 & -3360563.53 & 17646.90 & -2595023.94 & 14906169.12 & 4305381.76 \\ -5178963.69 & -976204.25 & 745716.11 & -2291577.37 & 4305381.76 & 27414097.24 \end{bmatrix} \tag{5.1}$$

was evaluated. In order to validated this result, the $\boldsymbol{P}$ matrix was verified to be positive definite and whether it would satisfy the LMI so that it becomes negative definite. This was carried out by determining the eigenvalues. The $\boldsymbol{P}$ matrix shows straight positive eigenvalues and the left hand-side of the linear matrix inequality negative ones.

Chapter 6

Discussion and Outlook

1. *Is it possible to design a FMPC for the rotor-craft model which performs well along the defined operation space?*
   Accordingly to the undertaking, a well performing FMPC could be designed. Therefore, under the principle of simplicity, an analogous model was utilized. The congruence of the characteristics of the two systems enabled this.
   Both systems have a main energy source for steady operation states. The additional two motor generators ensure a high efficiency factor due to the ability to store and provide energy in operation phases of excess and shortage. A rotatory spring-damper element is installed as an analogy of the original motor. Therefore, the elastic element was designed to be non-linear.
   For the design process, the proper operation range for the angular velocity of the rotational mass ω_4 depending on the required frequency spectrum was determined via a frequency analysis by the Bode plot. Within this range, the ν gap metric was applied to find an optimal partition for the above mentioned partition variable ω_4.
   Due to a too high number of operation points, simply the Euclidean metric was utilized. Within this procedure of backward regression a final number of 3 LLM was created which were rather aligned towards the right end of the operation space due to efficiency reasons. Therefore, the non-linear system was linearized in the operation points and a series of MPCs was designed.
   Finally, those MPCs are the foundation of the FMPC with output blending and trapezoidal membership functions with enable the interaction among each other and the non-linear model.
   An advantage of the trapezoidal membership function is that it allows the validity of each local linear model in the close vicinity of each operation point.
   Anyways, for the final analogous model the design process was carried out and an optimal setting of the sampling time, the predictive and control horizon and the

weighting matrices was found to ensure stability, no steady state errors, a sufficient damping and fast control behaviour for all the experiments in the individual operation region.
Finally, a disturbance suppression was implemented. Therefore, the FMPC could predicatively react to upcoming disturbances and enhance the robustness of the controller. Under the bottom line, it can be said that the predictive property of the FMPC, the possibility to design it on crucial interpolation points along the operation space, the ability to implement constraints on system variables and the predictive disturbance suppression legitimate to verify the research question of a robust FMPC.

2. *Does the implementation of inequality constraints allow feasible solutions for the FMPC?*
For the FMPC, two kinds of constraints were applied. The initially conceived hard constraints on the rotational speed of the combustion engine to ensure a reasonable efficiency factor did not effect the iterative solutions along the receding horizon. The necessity of implementing hard constraints on all system inputs arose later in the process of the simulation experiments.
However, the former output constraints did not restrict the solution space of FMPC along the time frame. The latter one did in deed have a noticeable impact. For the stationary phases, these hard constraints on the system input worked perfectly well. Yet, while transition between the local linear models a violation of those constraints could be observed.
The conclusion to be drawn here is that two phenomena play a crucial role on this. Firstly to be mentioned are off-equilibrium dynamics. Aggressive changes in the set-point signal along the transition stage lead to values of the state variable which would not have been reached otherwise. Hence, initially determined constraint solutions for one point in time might not overlap with behaviour of the non-linear system here.
The second phenomenon to mention is the superposition of the individual MPC by output blending. A more precise solution especially in the transition phase could be reached by parameter blending. So, the global cost function could be solved more satisfyingly under the contemplation of constraints. Yet, other disadvantages might occur here. A high level of experience and intuition for a control engineer is necessary here to balance advantages and disadvantages for the higher good of an efficient controller.
However, the implementation of inequality constraints for the FMPC only partially allow feasible solution.

3. *Can one show stability for this FMPC by the framework of Lyapunov?*
   The stability of the FMPC by Lyapunov requires a distinct knowledge of linear matrix inequalities. A set of prerequisites has to be fulfilled for a mathematical entity to be selected as a Lyapunov candidate. In the case of the stability proof by LMI, a suitable matrix has to be found for each linear matrix inequality which has to be positively defined. One of those considered matrices must fulfill the totality of LMI.
   For the Lyapunov candidate, the closed loop system matrix was chosen for which the open loop matrices and the MPC gain were permuted to mimic the transient behaviour of the FMPC among the local linear models.
   Anyhow, searching for a suitable matrix is a challenging task due to the wide range of the solution space. Therefore, a global search was carried out which led to a satisfying result. Yet, the configuration had to be slightly changed. The stability proof by Lyapunov for fuzzy systems deemed only a lower predictive horizon to be stable. However, a stability for this FMPC could be shown under some minor adjustments in its configuration.

Outlook

Within the scope of VARI-SPEED, a helicopter with a variable rotor speed was developed. The hybrid drive-train of a power turbine and a variator whose power exchange is done by continuous-variable transmission system enables this efficient operation behaviour.
In the scope of this master thesis a control design for the analogous model was carried out which was justified by the principle of similarity. Anyways, further developments in this direction shall be done. In this manner, the results of this thesis be applied for the original rotor-craft system. The scope of this undertaking can be enlarged to other types of helicopters as well. It is also conceivable to adapt these results of the control design to ordinary air-crafts. By taking further investigations into consideration, fruitful outcomes can result from this provided foundation.

Bibliography

[1] Hajek M. Pflumm T., Garre W. Vorhabenbeschreibung: Entwicklung eines drehzahlvariablen rotorsystems, 2015.

[2] Hajek M. Pflumm T., Garre W. Zwischenbericht i: Entwicklung eines drehzahlvariablen rotorsystems, 2015.

[3] Hajek M. Pflumm T., Garre W. Zwischenbericht ii: Entwicklung eines drehzahlvariablen rotorsystems, 2016.

[4] Hajek M. Pflumm T., Garre W. Zwischenbericht iii: Entwicklung eines drehzahlvariablen rotorsystems, 2017.

[5] Hajek M. Pflumm T., Rex W. Zwischenbericht iv: Entwicklung eines drehzahlvariablen rotorsystems, 2018.

[6] Hajek M. Pflumm T., Rex W. Abschlussbericht: Entwicklung eines drehzahlvariablen rotorsystems, 2019.

[7] Hajek M. Koch J., Reiser A. Zwischenbericht i: Antriebsstrangdynamik und flugeigenschaften von hubschraubern mit variabler hauptrotordrehzahl, 2018.

[8] Koch J. Poks A. Weigand M. Bischlaeger M., Gross C. Dynamic simulation of a rotor system with variable speed. 2022.

[9] Willem Rex, Tobias Pflumm, and Manfred Hajek. Uh-60a rotor and coupled rotor-fuselage simulation framework validation and analysis.

[10] Hanns Amri. *Variable rotor speed drivetrain investigation*. PhD thesis, Wien, 2018.

[11] Hanns Amri, R Feil, M Hajek, and Michael Weigand. Possibilities and difficulties for rotorcraft using variable transmission drive trains. *CEAS Aeronautical Journal*, 7:333–344, 2016.

[12] Hanns Amri, Roland Feil, Manfred Hajek, and Michael Weigand. übersetzungsvariable getriebe für drehflügler. In *63. Deutscher Luft-und Raumfahrt Kongress 2014*, page 14, 2014.

[13] Walter Bittner. *Flugmechanik der Hubschrauber: Technologie, das flugdynamische System Hubschrauber, Flugstabilitäten, Steuerbarkeit*. Springer-Verlag, 2014.

[14] Tobias Pflumm, Willem Garre, and Manfred Hajek. A preprocessor for parametric composite rotor blade cross-sections. 2018.

[15] Tobias Pflumm, Willem Rex, and Manfred Hajek. Propagation of material and manufacturing uncertainties in composite helicopter rotor blades. In *45th European Rotorcraft Forum*, 2019.

[16] Hyeonsoo Yeo, William G Bousman, and Wayne Johnson. Performance analysis of a utility helicopter with standard and advanced rotors. *Journal of the American Helicopter Society*, 49(3):250–270, 2004.

[17] Mark G Ballin. A high fidelity real-time simulation of a small turboshaft engine. Technical report, 1988.

[18] Dierk Schröder. *Elektrische Antriebe: Grundlagen*, volume 2. Springer, 1994.

[19] Antonio Visioli. A new design for a pid plus feedforward controller. *Journal of Process Control*, 14(4):457–463, 2004.

[20] Daniel S Christen. *Praxiswissen der chemischen verfahrenstechnik: handbuch für chemiker und verfahrensingenieure*. Springer-Verlag, 2009.

[21] Pierre Paschinger and Michael Weigand. Simulation of a compound-split transmission for the uh-60. In *44th European rotorcraft Forum*, page 11, 2018.

[22] Hanns Amri, TU Wien, Florian Donner, Felix Huber, and Michael Weigand. Mass optimisation of variable rotor speed compound split drivetrains for rotorcraft. tech. report, 45th European Rotorcraft Forum 2019, 2019.

[23] Pierre Paschinger, Hanns Amri, Katharina Hartentahler, and Michael Weigand. Compound-split drivetrains for rotorcraft. In *43rd European Rotorcraft Forum 2017*, page ERF2017_58, 2017.

[24] Stefan Jakubek Christoph Hametner. Zustandsregelung von mehrgrößensystemen. 2021.

[25] Stefan Enzendorfer. *Betrachtung von hybriden Antriebssträngen für Nutzfahrzeuge: Modellierung und Simulation eines seriellen Hybridbusses*. PhD thesis, 2009.

[26] Andrea Bonfiglio, Damiano Lanzarotto, Mario Marchesoni, Massimiliano Passalacqua, Renato Procopio, and Matteo Repetto. Electrical-loss analysis of power-split hybrid electric vehicles. *Energies*, 10(12):2142, 2017.

[27] Alexander Schirrer. *Efficient robust control design and optimization methods for flight control*. PhD thesis, 2011.

[28] Tor A Johansen and Bjarne A Foss. Operating regime based process modeling and identification. *Computers & chemical engineering*, 21(2):159–176, 1997.

[29] Roderick Murray-Smith, Daniel Sbarbaro, Carl Edward Rasmussen, and Agathe Girard. Adaptive, cautious, predictive control with gaussian process priors. *IFAC Proceedings Volumes*, 36(16):1155–1160, 2003.

[30] Wen-Hua Chen and Yi Cao. Stability analysis of constrained nonlinear model predictive control with terminal weighting. *Asian Journal of Control*, 14(5):1374–1381, 2012.

[31] Gregor Gregor**cic** and Gordon Lightbody. Nonlinear model-based control of highly nonlinear processes. *Computers & chemical engineering*, 34(8):1268–1281, 2010.

[32] Gregor Gregor**cic** and Gordon Lightbody. Nonlinear system identification: From multiple-model networks to gaussian processes. *Engineering Applications of Artificial Intelligence*, 21(7):1035–1055, 2008.

[33] Torsten Soderstrom and Petre Stoica. *System identification*. Prentice-Hall International, 1989.

[34] Hua O Wang and Kazuo Tanaka. *Fuzzy control systems design and analysis: a linear matrix inequality approach*. John Wiley & Sons, 2004.

[35] Lennart Ljung. *System identification*. Springer, 1998.

[36] Michaela Killian and Martin Kozek. Optimal partitioning of a boiler-turbine unit for fuzzy model predictive control. *IFAC-PapersOnLine*, 50(1):2011–2016, 2017.

[37] Roderik Murray-Smith and Henrik Gollee. A constructive learning algorithm for local model networks. In *Proceedings of the IEEE Workshop on Computer-Intensive Methods in Control and Signal Processing, Prague, Czech Republic*, pages 21–29, 1994.

[38] Roderick Murray-Smith and Kenneth Hunt. Local model architectures for nonlinear modelling and control. *Neural Network Engineering in dynamic control systems*, pages 61–82, 1995.

[39] Roderick Murray-Smith, Tor A Johansen, and Robert Shorten. On transient dynamics, off-equilibrium behaviour and identification in blended multiple model structures. In *1999 European Control Conference (ECC)*, pages 3569–3574. IEEE, 1999.

[40] Douglas J Leith and WE Leithead. Analytic framework for blended multiple model systems using linear local models. *International Journal of Control*, 72(7-8):605–619, 1999.

[41] Anass Boukhris, Gilles Mourot, and Jose Ragot. Non-linear dynamic system identification: a multi-model approach. *International Journal of Control*, 72(7-8):591–604, 1999.

[42] Kenneth J Hunt, JC Kalkkuhl, Hans Fritz, and Tor Arne Johansen. Constructive empirical modelling of longitudinal vehicle dynamics using local model networks. *Control Engineering Practice*, 4(2):167–178, 1996.

[43] Tor A Johansen and Bjarne Foss. Constructing narmax models using armax models. *International journal of control*, 58(5):1125–1153, 1993.

[44] Lukas Böhler, Jürgen Krail, Gregor Görtler, and Martin Kozek. Fuzzy model predictive control for small-scale biomass combustion furnaces. *Applied Energy*, 276:115339, 2020.

[45] Jingjing Du, Chunyue Song, and Ping Li. Application of gap metric to model bank determination in multilinear model approach. *Journal of Process Control*, 19(2):231–240, 2009.

[46] Wen Tan, Horacio J Marquez, Tongwen Chen, and Jizhen Liu. Analysis and control of a nonlinear boiler-turbine unit. *Journal of process control*, 15(8):883–891, 2005.

[47] Tryphon T Georgiou and Malcolm C Smith. Optimal robustness in the gap metric. In *Proceedings of the 28th IEEE Conference on Decision and Control,*, pages 2331–2336. IEEE, 1989.

[48] Yiguo Li, Jiong Shen, Kwang Y Lee, and Xichui Liu. Offset-free fuzzy model predictive control of a boiler–turbine system based on genetic algorithm. *Simulation modelling practice and theory*, 26:77–95, 2012.

[49] Ruiyun Qi, Gang Tao, and Bin Jiang. Fuzzy system identification and adaptive control. 2019.

[50] Kai Michels, Frank Klawonn, Rudolf Kruse, and Andreas Nürnberger. *Fuzzy-Regelung: Grundlagen, Entwurf, Analyse*. Springer-Verlag, 2013.

[51] Lotfi A Zadeh. Fuzzy sets. *Information and control*, 8(3):338–353, 1965.

[52] Tomohiro Takagi and Michio Sugeno. Fuzzy identification of systems and its applications to modeling and control. *IEEE transactions on systems, man, and cybernetics*, (1):116–132, 1985.

[53] Jay A Farrell and Marios M Polycarpou. *Adaptive approximation based control: unifying neural, fuzzy and traditional adaptive approximation approaches*. John Wiley & Sons, 2006.

[54] John H Lilly. *Fuzzy control and identification*. John Wiley & Sons, 2011.

[55] Dimiter Driankov and Rainer Palm. *Advances in fuzzy control*, volume 16. Physica, 2013.

[56] Tatjewski. *Advanced Control of Industrial Processes*. Springer-Verlag London Limited, 2007.

[57] Nicole Paces, Andreas Voigt, Stefan Jakubek, Alexander Schirrer, and Martin Kozek. Combined control of combustion load and combustion position in a moving grate biomass furnace. In *2011 19th Mediterranean Conference on Control & Automation (MED)*, pages 1447–1452. IEEE, 2011.

[58] Dawei Zhang, Zhiyong Zhou, and Xinchun Jia. Networked fuzzy output feedback control for discrete-time takagi–sugeno fuzzy systems with sensor saturation and measurement noise. *Information Sciences*, 457:182–194, 2018.

[59] Leung Lam. *Stability Analysis of Fuzzy-Model-Based Control Systems*, volume 1. Springer, 2011.

[60] Gang Feng. A survey on analysis and design of model-based fuzzy control systems. *IEEE Transactions on Fuzzy systems*, 14(5):676–697, 2006.

[61] Eduardo F Camacho and Carlos Bordons Alba. *Model predictive control*. Springer science & business media, 2013.

[62] Stefan Grosswindhager. *Modeling and control of biomass-fired district heating networks*. PhD thesis, 2013.

[63] Shaoyuan Li and Yi Zheng. *Distributed model predictive control for plant-wide systems*. John Wiley & Sons, 2016.

[64] Rainer Dittmar and Bernd-Markus Pfeiffer. *Modellbasierte prädiktive Regelung: Eine Einführung für Ingenieure*. Oldenbourg Verlag, 2004.

[65] David W Clarke, Coorous Mohtadi, and P Simon Tuffs. Generalized predictive control—part i. the basic algorithm. *Automatica*, 23(2):137–148, 1987.

[66] Liuping Wang. *Model predictive control system design and implementation using MATLAB®*. Springer Science & Business Media, 2009.

[67] Oliver König Stefan Jakubek, Alexander Schirrer. Adaptive und predictive control. 2020.

[68] Thomas Kailath. *Linear systems*, volume 156. Prentice-Hall Englewood Cliffs, NJ, 1980.

[69] Sohaib Aslam, Yew-Chung Chak, Mujtaba Hussain Jaffery, Renuganth Varatharajoo, and Ejaz Ahmad Ansari. Model predictive control for takagi–sugeno fuzzy model-based spacecraft combined energy and attitude control system. *Advances in Space Research*, 71(10):4155–4172, 2023.

[70] J. M. Maciejowski. *Predictive control. with constraints*. Pearson education, 2002.

[71] David Q Mayne, James B Rawlings, Christopher V Rao, and Pierre OM Scokaert. Constrained model predictive control: Stability and optimality. *Automatica*, 36(6):789–814, 2000.

[72] Julian Berberich, Johannes Köhler, Matthias A Müller, and Frank Allgöwer. Data-driven model predictive control with stability and robustness guarantees. *IEEE Transactions on Automatic Control*, 66(4):1702–1717, 2020.

[73] Manfred Morari and Jay H Lee. Model predictive control: past, present and future. *Computers & Chemical Engineering*, 23(4-5):667–682, 1999.

[74] J Anthony Rossiter, Basil Kouvaritakis, and MJ Rice. A numerically robust state-space approach to stable-predictive control strategies. *Automatica*, 34(1):65–73, 1998.

[75] S Keerthi and E Gilbert. Computation of minimum-time feedback control laws for discrete-time systems with state-control constraints. *IEEE Transactions on Automatic Control*, 32(5):432–435, 1987.

[76] Elmer G Gilbert and K Tin Tan. Linear systems with state and control constraints: The theory and application of maximal output admissible sets. *IEEE Transactions on Automatic control*, 36(9):1008–1020, 1991.

[77] Pierre OM Scokaert, David Q Mayne, and James B Rawlings. Suboptimal model predictive control (feasibility implies stability). *IEEE Transactions on Automatic Control*, 44(3):648–654, 1999.

[78] YL Huang, Helen H Lou, JP Gong, and Thomas F Edgar. Fuzzy model predictive control. *IEEE Transactions on Fuzzy Systems*, 8(6):665–678, 2000.

[79] János Abonyi and János Abonyi. *Fuzzy model identification*. Springer, 2003.

[80] Robert Babu*s*ka. *Fuzzy modeling for control*, volume 12. Springer Science & Business Media, 2012.

[81] S Mollov, P van den Veen, R Babuska, J Abonyi, J Roubos, and H Verbruggen. Extraction of local linear models from takagi-sugeno fuzzy model with application to modelbased predictive control eufit, 1999. *Aachen, Germany*.

[82] Yong Wang, Qiangang Zheng, Haibo Zhang, and Haoying Chen. Study on inversion control for integrated helicopter/engine system with variable rotor speed based on state variable model. *International Journal of Turbo & Jet-Engines*, 40(1):21–29, 2023.

[83] Yong Wang, Kaiming Huang, Yerong Peng, Jie Song, and Haibo Zhang. Design and test of adaptive torsional vibration suppression method for helicopter power system with variable rotor speed. *Proceedings of the Institution of Mechanical Engineers, Part I: Journal of Systems and Control Engineering*, 236(7):1324–1334, 2022.

[84] Yong Wang, Qiangang Zheng, Haibo Zhang, and Haoying Chen. Research on predictive control of helicopter/engine based on lms adaptive torsional vibration suppression. *Journal of Low Frequency Noise, Vibration and Active Control*, 37(4):1151–1163, 2018.

[85] Yong Wang, Qiangang Zheng, Dawei Fu, and Haibo Zhang. Study on adaptive torsional vibration suppression methods for helicopter/turboshaft engine system with variable rotor speed. *Asian Journal of Control*, 23(3):1490–1502, 2021.

[86] Yong Wang, Qiangang Zheng, Haibo Zhang, and Yuan Gao. A study on nonlinear model predictive control for helicopter/engine with variable rotor speed based on

linear kalman filter. *International Journal of Turbo & Jet-Engines*, 39(3):357–366, 2022.